Research Square

Preprints are preliminary reports that have not undergone peer review.
They should not be considered conclusive, used to inform clinical practice,
or referenced by the media as validated information.

Metal–Organic Framework/Silver Hybrid Nanocomposite Membrane with Layer-by-Layer Architecture for mixture gas and dye separation

Prarthana Bora
CSIR-NEIST: North East Institute of Science and Technology CSIR
Ankur Jyoti Bhuyan
CSIR-NEIST: North East Institute of Science and Technology CSIR
Chinmoy Bhuyan
CSIR-NEIST: North East Institute of Science and Technology CSIR
Priyadarshini Gogoi
CSIR-NEIST: North East Institute of Science and Technology CSIR
Xianshe Feng
University of Waterloo Faculty of Engineering
Swapnali Hazarika
shrrljt@yahoo.com

CSIR-NEIST: North East Institute of Science and Technology CSIR https://orcid.org/0000-0002-4839-3566

Research Article

Keywords: ZIFs, porous materials, silver, mixed matrix membrane, gas separation, Knudsen diffusion, Polyvinyl chloride

Posted Date: November 13th, 2026

DOI: https://doi.org/10.21203/rs.3.rs-11433043/v1

License: This work is licensed under a Creative Commons Attribution 4.0 International License.
Read Full License

Metal–Organic Framework/Silver Hybrid Nanocomposite Membrane with Layer-by-Layer Architecture for mixture gas and dye separation

Prarthana Bora[a,b], Ankur Jyoti Bhuyan[a,b], Chinmoy Bhuyan[a,b], Priyadarshini Gogoi[a,b], Xianshe Feng[c], Swapnali Hazarika[a,b]*

[a]Centre for Petroleum Research and Chemical Engineering Group, Chemical Sciences and Technology Division, CSIR-North East Institute of Science and Technology, Jorhat – 785006, Assam, India

[b]Academy of Scientific and Innovative Research (AcSIR), Ghaziabad-201002, India

[c]Department of Chemical Engineering, University of Waterloo, Waterloo N2L 3G1, Canada

*Author for correspondence

Phone: +913762370012, Email: shrrljt@yahoo.com

Abstract:

Porous filler incorporation in polymer matrix is one of the most effective ways to enhance permeability, separation efficiency, thermal-mechanical stability and fouling resistance of a membrane. Zeolitic imidazolate framework (ZIF) is a potential class of porous material which can be used in gas separation membranes due to the advantages of small pore aperture and excellent thermal and chemical stability. Herein, we report a Mixed Matrix Membrane developed by incorporating Ag-doped bimetallic ZIF-8 nanoparticles into a polyvinyl chloride/polyethylene glycol diamine (PVC/PEGdiamine) matrix via simple blending method. To boost the selectivity, a thin layer of chitosan crosslinked with silver was laminated on the blend membrane. The structural and chemical properties of the materials and membranes were well characterized via sophisticated analytical tools. In addition to the tunable porous architecture of the modified ZIF-8, this synergistic design provides enhanced interfacial compatibility and defect suppression. The gas permeance measurements of the constructed membranes for a wide range of gases viz., H_2, N_2, O_2, C_2H_4 and C_2H_6 revealed a maximum H_2/N_2 selectivity of 3.2 while selectivities obtained for other gas pairs O_2/N_2 and C_2H_4/C_2H_6 remained comparatively very low, indicating the transport was predominantly governed by Knudsen diffusion. The highest H_2 permeance exhibited by the fabricated MMM is 6258 GPU. The MMM showed a water flux of 58.2 $L.m^{-2}.h^{-1}$ with a 69.7% rejection of MB dye aqueous media. The adsorptive behaviour of ZIF-8@Ag and size sieving property of the membrane participate simultaneously in effective removal of the MB dye from aqueous solution.

Keywords: ZIFs, porous materials, silver, mixed matrix membrane, gas separation, Knudsen diffusion, Polyvinyl chloride

Abbreviations:

Abbreviations	Full forms
MMMs	Mixed matrix membranes
MOF	Metal organic framework
CNT	Carbon nanotube
CMS	Covalent organic framework
POC	Porous organic cage
ZIFs	Zeolitic imidazolate framework
MB	Methylene blue
PVC	Polyvinyl chloride
PEGdiamine	Polyethylene glycol diamine
FTIR	Fourier Transform Infrared (spectroscopy)
XRD	X-Ray Diffraction
FESEM	Field Emission Scanning Electron Microscope
UV	Ultraviolet
rpm	Rotation per minute
DMF	N,N-Dimethylformamide
GPU	Gas Permeation Unit
STP	Standard Temperature and Pressure

Acknowledgements:

Fundings: S Hazarika thanks CSIR New Delhi for CSIR Mission Mode Project grant MMP065202, P. Bora and P. Gogoi thank Department of Science and Technology, Government of India for INSPIRE fellowship (grant no. IF200403 (GAP0811) and IF240080 (GAP0851)). C. Bhuyan thanks Council of Scientific & Industrial Research, New Delhi, India for Senior Research Fellowship (Direct) (ID No. 35110313). A. J. Bhuyan acknowledge Numaligarh Refinery Ltd., Assam for the research grant GPP-0439.

Grants: Authors acknowledge Department of Chemicals and Petrochemicals, Ministry of Chemicals and Fertilizers, Government of India for the research grant GPP0373; CSIR New Delhi for CSIR Mission Mode Project grant MMP065202.

People: Authors thank Director CSIR-NEIST, Jorhat for encouraging the research group during various discussions.

1. Introduction

Membranes outstand as a phenomenal branch of separation and purification technology owing to the advantageous properties of energy efficiency, cost effectiveness, large scale up scope, simple handling and high separation efficiency (Alomar et al. 2026a; Bora et al. 2023; Bora et al. 2026; Bhuyan et al. 2025). The tunable nature of membrane provides tremendous scopes for tailoring their pores and surface functionality, as required by the application. Research on gas separation membranes has been growing day by day with respect to the demand for high purity gases in various applications. H_2, O_2 and low molecular weight olefins are such demanding gases that needed in highly pure form (Tian et al. 2025; Patil et al. 2023; Zhang et al. 2025). Membrane technology has been used widely in gas separation applications. Most of the membranes used for gas separation at commercial level are polymeric membranes. Conventional polymeric membranes often face several issues in gas separation such as permeability-selectivity trade-off, swelling of polymer, plasticization, ageing etc. These issues limit the use of polymeric membranes in harsh conditions for prolonged time. Introduction of selective filler materials in membrane structure has been proved as one of the most effective ways to mitigate these issues related to conventional membranes (Niu et al. 2024). Filler incorporation produces a new class of membrane called mixed matrix membranes (MMMs) which possess excellent physicochemical stability, good selectivity and permeability. Filler materials can be defined as the dispersed phase which are added to continuous polymer matrix to introduce superior properties. Fillers can be divided into various types such as inorganic fillers, carbon-based fillers, porous fillers etc. Zeolite (Adams et al. 2011), metal organic framework (MOF) (Basu et al. 2011), carbon nanotube (CNT) (Ismail et al. 2011) , carbon molecular sieve (CMS) (Vu et al. 2003), nanocellulose (Bora et al. 2023) etc. are some examples of filler materials that have been reportedly used as dispersed phase in various membranes for gas separation application. Incorporation of inorganic fillers in polymeric membrane integrates the advanced properties of fillers such as molecular adsorption and diffusion capacity with the advantageous properties of polymeric membranes such as good processability and scalability (Ul Haq et al. 2021). Although various filler materials have been reportedly used in gas separation application, porous materials are excellent branch of inorganic materials having tremendous opportunity due to their high porosity, high surface area, good compatibility with polymer, excellent thermal and mechanical stability. The mostly reported porous materials are MOF, covalent organic framework (COF), porous organic cages (POC) etc. Out of these porous materials, MOFs, especially zeolitic imidazolate frameworks (ZIFs) have found enormous interest in the field of gas separation (Khan et al. 2026). ZIFs are promising class of MOFs constructed with metal cations and organic linkers. Most commonly used ZIF is ZIF-8 where the Zn transition metal is interconnected with imidazole linkers. ZIF-8

nanoparticle shows high surface area, excellent thermal and chemical stability with a small pore aperture of 3.4 Å (Park et al. 2006).

While incorporating nanofillers in membrane matrix, achieving homogeneous distribution is challenging. This difficulty can be solved by modification of nanomaterials via foreign materials/functionality inclusion to enhance their compatibility with other membrane materials such as polymers. Various functionalization of ZIF-8 have been carried out in order to enhance permeability of a specific gas. For example, amine functionalization of ZIF-8 is often observed for increasing CO_2 permeability (Zhao et al. 2024; Jiao et al. 2021). Reportedly, ZIF-8 membranes have also been effectively used for H_2 separation (Shan et al. 2023). The pore aperture of ZIF-8 is favourable for allowing permeation of small gas molecules like H_2 (2.89 Å) and O_2 (3.46 Å). Silver (Ag) doped ZIF-8 has been reported in a few literature where it shows profound application in the field of photocatalysis (Abdi 2020), electrocatalysis (Usman and Suliman 2023), adsorption (Chen et al. 2019), water purification (Rodriguez et al. 2023), and gas separation (Li et al. 2025). Ag incorporation in ZIF-8 is found to be successful in the field of gas separation, mostly in olefin paraffin separation, as Ag can facilitate the transport of olefin over paraffin. Peng et al. (2023) have synthesized of Ag/ZIF-8 based MMM and successfully implemented in propylene/propane separation. The membrane has exhibited highest propylene permeability of 3767 Barrer with an ideal selectivity of 11.7.

Clean water scarcity is another burning issue of present time which has been escalating day by day (Alomar et al. 2026b). Dye is a common water contaminant generally produced in various industrial sectors. Reportedly, ZIF-8 act as a very good adsorbent material for dyes (Liu et al. 2018). ZIF-8 can participate in electrostatic and π–π stacking interaction with ionic and aromatic ring containing dyes respectively, thereby achieving good adsorption as well as rejection efficiency (Liu et al. 2018; Sutrisna et al. 2026). Sutrisna et al. (2026) have reported a ZIF-8 and GO incorporated cellulose acetate based MMM which achieved 99.7% removal of methylene blue (MB) dye. Another study has reported the use of ZIF-8 in membrane fabrication for effective RhB dye separation (Liu et al. 2025).

The state of the art techniques for nanomaterial incorporated membrane synthesis are blending (Shi et al. 2021), cross-linking (Dilshad et al. 2021), and surface coating via interfacial polymerization (Niu et al. 2022), spray coating (Zakaria et al. 2026), spin coating (Geng et al. 2024) etc. The coating processes provide thin selective layer which minimizes over-all defect in the membrane. However, in terms of simplicity and scalability, blending is more advantageous. Cross-linking not only boost the membrane stability by increasing interfacial compatibility but also enhance membrane's selectivity and permeability (Wijenayake et al. 2013; Ji et al. 2026). Most importantly, cross-linking helps the membrane in tackling so called plasticization effect commonly observed in

polymeric gas separation membranes. In this study a membrane with layer by layer architecture has been synthesized where different stages of membrane modification includes blending, cross-linking as well as surface coating. Firstly, a silver doped ZIF-8 (ZIF-8@Ag) incorporated cross-linked MMM has been synthesized via simple blending process. The ZIF-8@Ag nanoparticle is incorporated in a polyvinyl chloride/ polyethylene glycol diamine (PVC/PEGdiamine) matrix, where PEGdiamine act as a cross-linker which bind PVC and ZIF-8@Ag in a single configuration. PVC is known for its low cost, durability and good chemical stability. However, in the field of gas separation it offers high selectivity at the expense of low permeability (Khalilinejad et al. 2015; Ahmadpour et al. 2014). To improve the gas permeability of pristine PVC membranes, various modifications have been attempted till date (Noorani and Mehrdad 2019). Modification of PVC with 1-vinylimidazole (Noorani and Mehrdad 2020), poly(1–vinylimidazole) (Noorani and Mehrdad 2019), poly (ether-6-block amide) (Khalilinejad et al. 2015), poly(amide-6-b-ethyleneoxide) (Ahmadpour et al. 2014), poly (methacrylic acid) (Wang 2021) etc. are reported aiming improved gas transport properties. Introduction of polyethylene glycol diamine (PEGdiamine) in PVC matrix via optimized blending is a novel concept as the amine's groups of PEGdiamine can interact with PVC to provide a strong yet flexible architecture. Shin et al. (2017) have reported a PVC- poly(oxyethylene methacrylate) graft copolymer membrane incorporated with ZIF-8 nanoparticle aiming CO_2/CH_4 separation. Another study has reported the combination of PVC with ZIF-8 which is further modified with layered double hydroxide and polyethyleneimine (Shariatmadari et al. 2023). However, the combination of PVC with Ag doped ZIF-8 is very few which mainly focuses on desalination and antibacterial performances (El-Sawaf et al. 2024; Hashem et al. 2023; Hashem 2023). More precisely, the PEGdiamaine modified PVC and ZIF-8@Ag based membrane have not been explored till date in the field of gas as well as dye separation.

Another thin layer of silver crosslinked chitosan has been coated on the PVC/PEGdiamine/ZIF-8@Ag MMM to study the impact of additional chitosan/Ag^+ layer on membrane performance. Chitosan is well known for its low cost, non-toxicity, biodegradability and excellent film forming ability (Xu et al. 2008). Due to its rich functionality, chitosan-based membrane are found to be highly applicable in gas separation membranes (Katare et al. 2023). Incorporation of Ag (I) in chitosan membrane has been reported in many literatures aiming gas separation (Zhang et al. 2025; Min et al. 2024). However, combination with PVC/PEGdiamine/ZIF-8@Ag MMM is still not endeavoured. The aim of this work was to find out how each layer affects gas and water transport. The single-gas permeances of H_2, N_2, O_2, C_2H_4 and C_2H_6 were measured after each step and at three ZIF-8@Ag loadings, ideal selectivity were calculated. Moreover, the applicability of the fabricated membrane in water treatment has also been tested using methylene blue dye as contaminant.

2. Experimental

2.1. Materials

$Zn(NO_3)_2.6H_2O$ (CAS no. 10196-18-6), sodium hydroxide NaOH (CAS no. 1310-73-2) and N,N-Dimethylformamide (DMF) (CAS no. 68-12-2) used in this study were purchased from Sisco Research Laboratories Pvt. Ltd. (India). 2-methylimidazole (CAS no. 693-98-1) and polyvinyl chloride PVC (CAS no. 9002-86-2) were purchased from Central Drug House (P) Ltd. Silver nitrate (CAS no. 7761-88-8) and Poly(ethylene glycol) diamine (Average M_N = 3000 g/mol, CAS no. 24991-53-5) were purchased from Sigma-Aldrich (India). Chitosan (CAS no. 9012-76-4) was purchased from Tokyo Chemical Industries Co. Ltd. (Japan). Methanol (CAS no. 67-56-1) and acetic acid glacial (CAS no. 64-19-7) were purchased from RFCL Limited (India) and Avantor Performance Materials India Limited respectively. Methylene blue (MB) dye is obtained from Sisco Research Laboratories Pvt. Ltd. (SRL), India.

2.2. Characterizations

FTIR analysis of the materials and membranes were confirmed by Perkin Elmer FTIR instrument, and all the analysis are conducted in ATR mode. The structure, surface and cross-sectional morphology of the synthesized materials and membranes were done via field emission scanning electron microscope (FESEM) (Model: JEOL JSM-IT710HR, Japan) and Carl Zeiss Sigma VP Field Emission Scanning electron microscope. Energy dispersive X-ray spectroscopy (EDX) integrated with the FESEM instrument was employed for elemental composition analysis. The elemental distribution in the synthesized materials and membranes was done via XPS analysis with a Thermo Fisher Scientific ESCALAB Xi+ instrument. The tensile property of the membranes was tested by using universal testing machine ("Tinius Olsen 5ST" model) having a load cell of capacity 5 kN. The surface roughness of the membranes is analysed by an AFM Nanomagnetics' hpAFM analyzer. Thermal stability of the membrane has been analyzed using Perkin Elmer 4000 instrument in a temperature range of 35 − 700 ºC with heating rate of 10 ºC/min in N_2 environment. BET analysis of the synthesized materials and membranes were done by BET analyzer (Quantachrome Instruments version 5.21). For BET analysis, nitrogen gas and outgas temperature of 150 ºC was used. XRD analysis of the materials was done using X-ray diffractometer manufactured by Bruker (Model: D6 Phaser). Water contact angle measurement of the membranes was analysed via a contact angle analyzer (Model: DM-501, Kyowa Interface Science Co. Ltd.). A UV visible spectrophotometer (Model No. : UV-2600I, SHIMADZU) is employed for determining the concentration of feed solution and permeate.

2.3. Synthesis of ZIF-8 nanoparticle

ZIF-8 nanoparticle has been synthesized via a reported method (Figure 1a) (He et al. 2024). Firstly, 3g of $Zn(NO_3)_2.6H_2O$ (10 mmol) was added to MeOH (140 mL) solution and dissolution is attained via mechanical

stirring. Under vigorous stirring, a solution of 6.60g 2-methyl imidazole (80.39 mmol) in 140 mL MeOH has been added to the solution of $Zn(NO_3)_2.6H_2O$. The mixed solution was stirred for 24 hours at room temperature. Collection of the resultant product was done through centrifugation at 8000 rpm (15 min). The product is washed three times with MeOH to ensure the removal of unreacted starting materials. The resultant product is allowed to dry in a hot air oven for 12 hours at 60 ºC. The white powdery product of ZIF-8 is stored for further use.

2.4. Synthesis of ZIF-8@Ag nanoparticle

To synthesize Ag doped ZIF-8 bimetallic nanoparticle a simple method has been adopted (Barjasteh et al. 2023). A solution of pre-synthesized ZIF-8 nanoparticle in MeOH (0.228g in 20mL) is prepared. Another 10 mL solution of 0.170 g silver nitrate (1:1 molar ratio of Ag:Zn) is prepared in MeOH. Both the solutions were kept in ice-water bath for 10 min. The silver nitrate solution is poured slowly in the ZIF-8 solution and stirred further for 30 min in the ice bath while maintaining the temperature ~ 0 ºC. During this process ion exchange takes place between Ag^+ and Zn^{2+} ions owing to the ability of Ag^+ to form complexation with 2-methylimidazole. As a result, a pale white product is formed which was collected via centrifugation, followed by several washes with methanol. The resultant product is dried at 60 ºC for 12 hours in a hot air oven and stored for further use.

2.5. Synthesis of PVC-PEGdiamine membrane

Two polymers PVC and PEGdiamine are used to fabricate the support membrane via non-solvent induced phase separation (NIPS) technique. PEGdiamine is utilized as a modifier in PVC to enhance the stability of the support membrane. 14g of PVC is dissolved in 90 mL of DMF (85 g) via vigorous stirring at 70 ºC for 12 hours. After attaining proper dissolution, at same temperature condition, 1g of PEGdiamine is added and stirred further for 4 hours at 80 ºC. The bubble free polymer blend solution is cast over a clean glass plate with a glass rod maintaining uniform thickness. After a min of evaporation, the glass plate is immersed in a water bath for 12 hours for the solvent exchange to occur. The membrane obtained is again placed in a fresh water bath for removal of the residual solvent. M-0 membrane is dried at 60 ºC and used for further study.

2.6. Synthesis of ZIF-8@Ag incorporated membrane

Incorporation of ZIF-8@Ag nanoparticle has been done via blending with polymers during the dope solution preparation phase prior to membrane fabrication. First, 1 wt. % ZIF-8@Ag nanoparticle (1g) in DMF is sonicated for 1 hour in an ultrasonic bath. The dispersed nanoparticle is then added to the PVC/PEGdiamine (14 g/1 g) blend solution, while maintaining the total solvent (DMF) amount of 84 g in the mixture. The nanoparticle incorporated dope solution is allowed to stir for 2 hours at ambient temperature to attain a homogeneously dispersed solution. The PEGdiamine may act as a crosslinker to link PVC and ZIF-8@Ag in a single stable platform. The MMM (M-

AZ) has been obtained by NIPS technique as described in earlier section. The ZIF8@Ag concentration in the membrane are varied as 0.5, 1 and 1.5 wt. %.

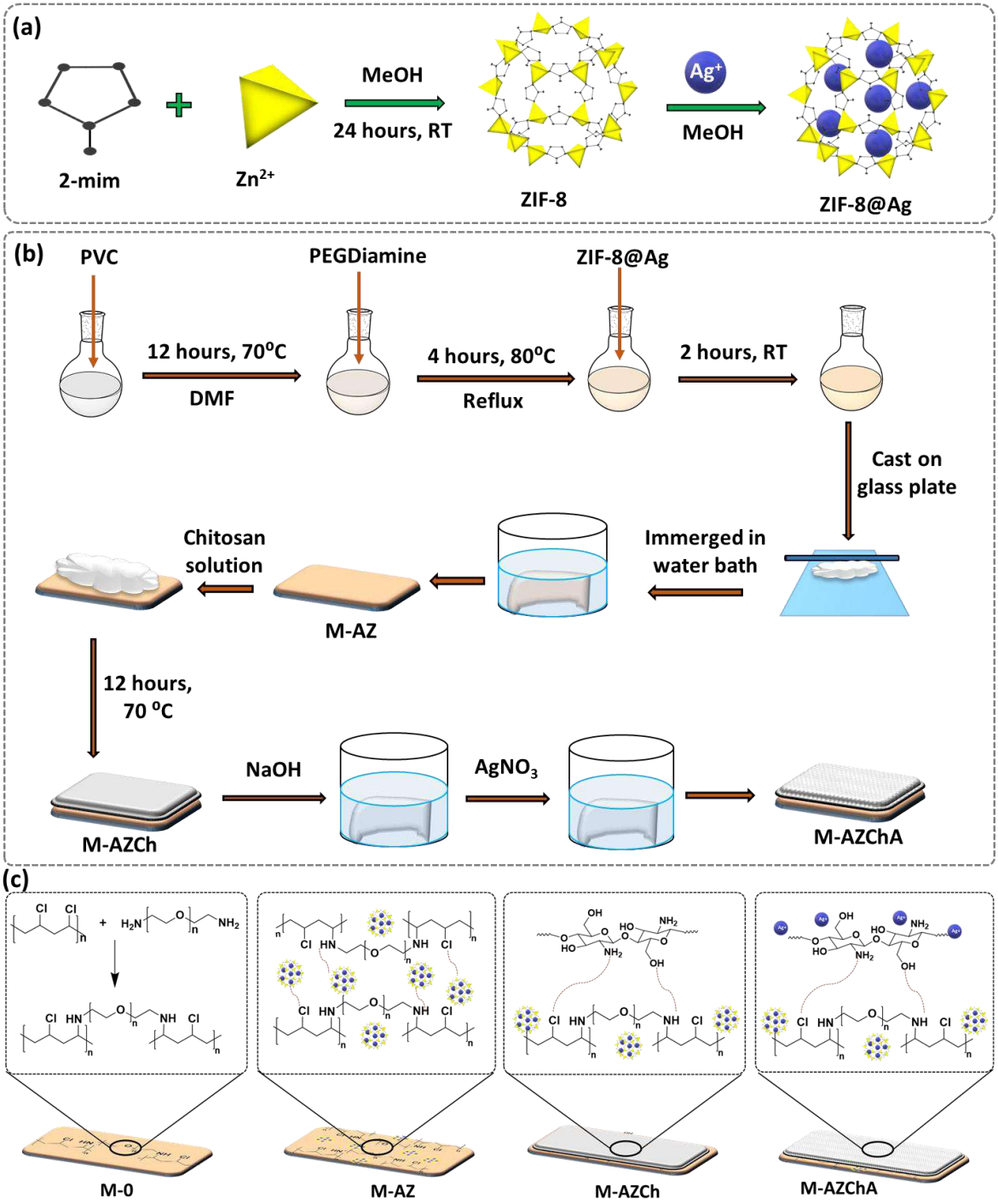


Figure 1: (a) Synthesis route of ZIF-8 and ZIF-8@Ag, (b) Different steps involved in membrane fabrications and (c) interactions present inside the fabricated membranes

2.7. Synthesis of chitosan/Ag^+ crosslinked membrane

To boost selectivity, an additional layer of chitosan/Ag^+ has been coated over the blend M-AZ membrane. First, a 1.6 wt. % chitosan in acetic acid solution (0.5 M) has been prepared. The chitosan solution is spread over the M-AZ membrane with a glass rod followed by 12 hours of heat treatment at 70 ºC in a hot air oven to ensure a stable coating. M-AZCh membrane is immersed in a NaOH (0.5M) solution to remove the remaining acetic acid. This process further converts the protonated $–NH_3^+$ of chitosan to neutral $–NH_2$ form. The membrane is then immersed in an aqueous solution of 1 M $AgNO_3$ solution for 2 hours. The M-AZChA membrane is air dried and stored for gas separation application.

The composition of the fabricated membranes is given in Table 1. The stepwise fabrication of membranes and the plausible interactions that may take place inside the membranes at various steps are presented in Figure 1b and 1c respectively. Reportedly, nitrogen in amine groups can act as a nucleophile and efficiently bind with PVC backbone (Ameer et al. 2013). This results in partial amination of PVC backbone, which further leads to chemical cross-linking among the polymer chains. After incorporation of ZIF-8 in the PVC-PEGdiamine matrix, it may introduce different types of interactions within the membrane matrix such as van der Waals interaction, dipole-dipole interactions etc. Additionally, Zn^{2+} and Ag^+ sites of ZIF-8@Ag can coordinate with amine groups of PEGdiamine via Lewis acid base interaction (Jo et al. 2022). These interactions further improve the filler dispersion in the polymer matrix. After chitosan layer deposition, the inherent amine, hydroxyl and carbonyl groups of chitosan can interact with exposed PVC, PEGdiamine as well as ZIF-8 on the MMM surface. After immersion of the membrane in $AgNO_3$ solution, the functional groups present in chitosan participate actively to coordinate with Ag^+ making another crosslinked layer of chitosan/Ag^+ (Min et al. 2024).

Table 1: Compositions of different components in the fabricated membranes

Abbreviation	**PVC (g)**	**PEG diamine (g)**	**DMF (g)**	**ZIF-8@Ag (AZ) (g)**	**Chitosan (Ch) (wt.%)**	**$AgNO_3$ (A) (M)**
M-0	14	1	85	-	-	-
M-AZ	14	1	84	1	-	-
M-AZCh	14	1	84	1	1.6	-
M-AZChA	14	1	84.5	0.5	1.6	1
			84	1		
			83.5	1.5		

2.8. Gas separation experimental procedure

At room temperature, pure gas permeation experiment of different gases (H_2, N_2, O_2, C_2H_6 and C_2H_4) are done. A membrane with effective area of 23.8 cm^2 is mounted in the permeation cell (Figure 2). The feed gas was subjected in the membrane cell at a given feed pressure while the permeate side is maintained at atmospheric pressure (Experimental conditions are tabulated in Table S1 of Supplementary Materials). The permeation rate of gases through the membrane from feed to permeate side was assessed with the help of a soap bubble flow meter and the gas concentrations were measured using gas chromatography (GC) (Figure 2). The permeation rate of the gases are measured in terms of gas permeance using Equation 1.

$$P = \frac{Q}{A\Delta p} \qquad (1)$$

Here, P represents gas permeance, Q signifies volumetric permeation rate at standard condition (STP), Δp and A represents the pressure difference across the membrane effective area of the membrane used for permeation experiment. The gas permeance is expressed in Gas permeation unit (GPU) where 1 GPU = 10^{-6} cm^3(STP)/cm^2.s.cmHg.

Ideal selectivity of the membranes to a gas pair was measured in terms of pure gas permeance ratio by using Equation 2.

$$\text{Selectivity (i/j)} = \frac{P_i}{P_j} \qquad (2)$$

Here, Pi and Pj represent pure gas permeance of i and j gases respectively to obtain selectivity of i/j gas pair.

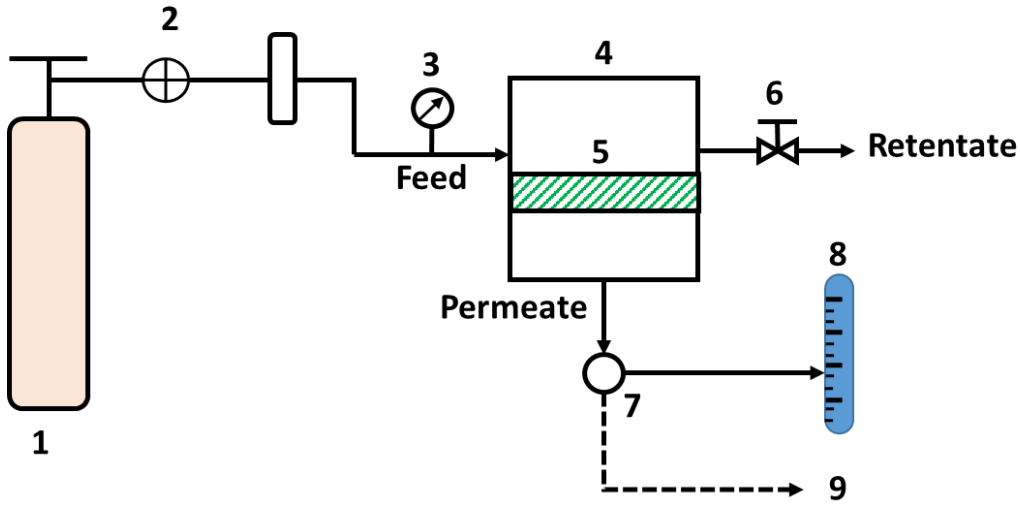


Figure 2: Schematic representation of permeation set up; 1: Gas cylinder, 2: Pressure regulator, 3: Pressure gauge, 4: Permeation cell, 5: Membrane, 6: valve, 7: 3-way valve, 8: Bubble flowmeter, 9: GC

3. Results and discussion

3.1. Characterization of synthesized materials

FTIR analysis of ZIF-8 and ZIF-8@Ag exhibited peaks at 2984 cm^{-1} represent C-H stretching vibration (Figure 3a) (Sultana et al. 2024; Khajavian et al. 2020). Characteristic peaks at ~1576 cm^{-1} in both the materials arises because of the C=N stretching vibration. Peaks at 1137 cm^{-1}, 991 cm^{-1}, 758 cm^{-1} and 697 cm^{-1} can be attributed to C-N stretching vibration, C-N bending vibration, C-H bending vibration and imidazole ring's out of plane bending vibration respectively (Zhang et al. 2018). Two peaks at 1424 cm^{-1} and 1311 cm^{-1} indicates the existence of aromatic imidazole ring (Ravinayagam and Rehman 2020). XRD analysis of ZIF-8 and ZIF-8@Ag were conducted to analyse the crystalline nature of the materials. ZIF-8 showed XRD pattern in accordance to the literature (Figure 3b) (Abdi 2020). Well defined intense peaks in XRD pattern of ZIF-8 has been observed with 2Θ values of 7.33º, 10.24º, 12.69º, 14.7º, 16.49º, 18.06º, 22.08º, 24.31º and 26.54º corresponds to the diffraction planes of 011, 002, 112, 022, 013, 222, 114, 233 and 134 respectively (Yang et al. 2018). This observation reveals that the synthesized material ZIF-8 have high crystallinity with a sodalite type structure. From the XRD pattern of ZIF-8@Ag, the major peaks of ZIF-8 are observed to be remained intact with no sign of impurity. Lowering of peak intensity has been observed in ZIF-8@Ag which reveals the partial loss of crystallinity after effective integration of Ag in ZIF-8 (Abdi 2020). Pore size distribution analysis of ZIF-8 and ZIF-8@Ag have been measured via BET analysis and the obtained graphs are presented in Figure 3c and 3d respectively. From the pore size distribution graphs of both the materials it is observed that maximum pores fall in the range of ~10-30 Å. However, careful observation reveals that maximum pores shift toward lower pore size region after silver incorporation, which can be explained from the filling of free sites present in ZIF-8 cavity by Ag species. This is further validated by the change in surface area of ZIF-8 from 1641.421 m^2/g to 923.691 m^2/g after Ag incorporation.

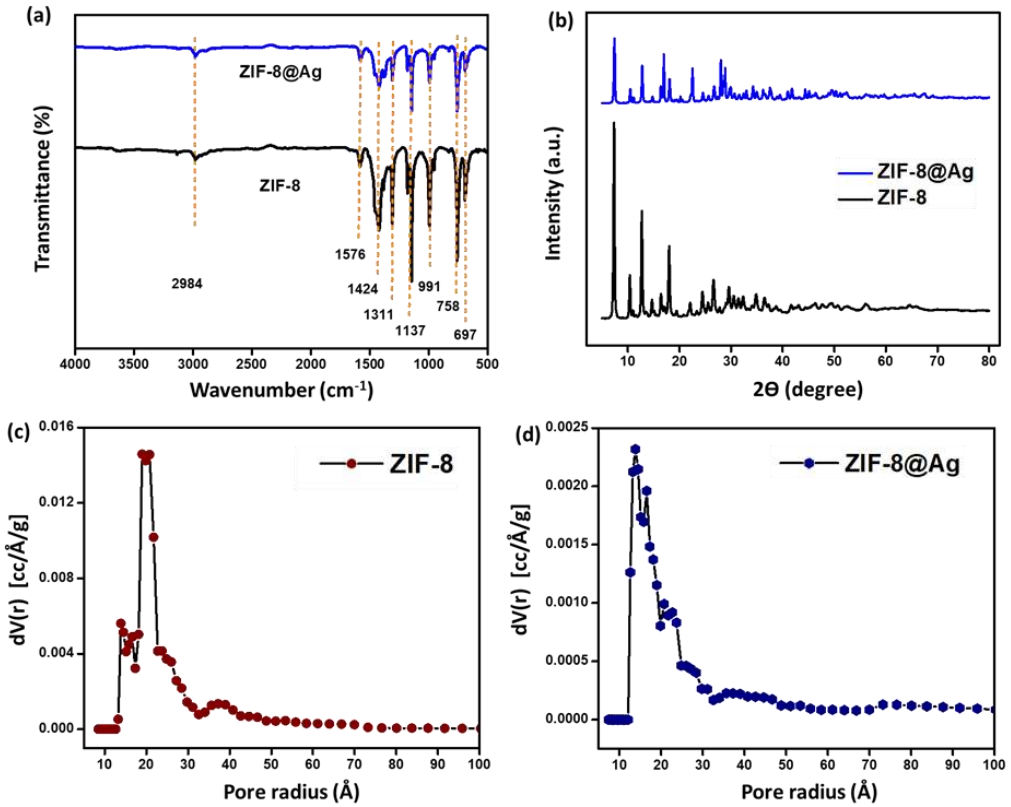


Figure 3: (a) FTIR spectra and (b) XRD pattern of ZIF-8 and ZIF-8@Ag; Pore size distribution graph of (c) ZIF-8 and (d) ZIF-8@Ag

XPS analysis of the synthesized materials provides insights into the binding environment of different elements present inside. The survey spectra of ZIF-8, provided in Figure 4a showed respective peaks for C1s, N1s and Zn2p which forms the ZIF-8 architecture. After modification with Ag, ZIF-8@Ag showed additional peak for Ag3d in its survey spectra (Figure 4b). To gain deeper understanding of the bonding of individual elements, deconvolution of the corresponding high resolution peaks of ZIF-8 and ZIF-8@Ag were done and presented in Figure 4c and Figure 4d respectively. C1s spectra of both the materials showed two peaks, one at lower and another at higher binding energy which indicates C-C/C-H and C-N/C=N bindings present in the imidazole ring respectively (Papurello et al. 2019). Zn2p deconvolution spectra of ZIF-8 and ZIF-8@Ag showed the characteristic peaks for $Zn2p_{1/2}$ and $Zn2p_{3/2}$ at ~1045 eV and ~1022 eV respectively which obtained as a result of spin orbit coupling (Tian et al. 2025). N1s deconvolution spectra showed peaks for N-C and N-Zn in both the materials. In ZIF-8@Ag, deconvolution spectra of Ag3d exhibited two distinctive peaks at 374.2 eV and 368.3 eV which corresponds to core energy levels of $Ag3d_{3/2}$ and $Ag3d_{5/2}$ respectively originates mainly from spin-orbit coupling of Ag3d (Parashar and Komarala 2017).

FESEM analysis of ZIF-8 and ZIF-8@Ag are conducted to evaluate the particle size, shape and morphology. From Figure 5a.1 and 5a.2, sodalite like structure of ZIF-8 particles confirmed its successful synthesis. ZIF-8 particles are distributed in 50-500 nm range cubic shaped crystal morphology. After modification with Ag, the crystalline structure of ZIF-8 changes noticeably. Incorporated Ag can create partial lattice disorder and generate defects which may cause the reduction in long range crystallinity of ZIF-8. From Figure 5b.1 and 5b.2, changes in crystalline characteristics indicate partial loss of crystallinity rather than complete amorphization. This observation is consistent with the results obtained from XRD. EDX analysis of ZIF-8@Ag provided in Figure S3 of Supplementary Materials also validates the incorporation of Ag. The atomic percentage of Ag in ZIF-8@Ag is found to be 0.40 % along with C (51.18%), N (46.81%) and Zn (1.61%) (Table S2).

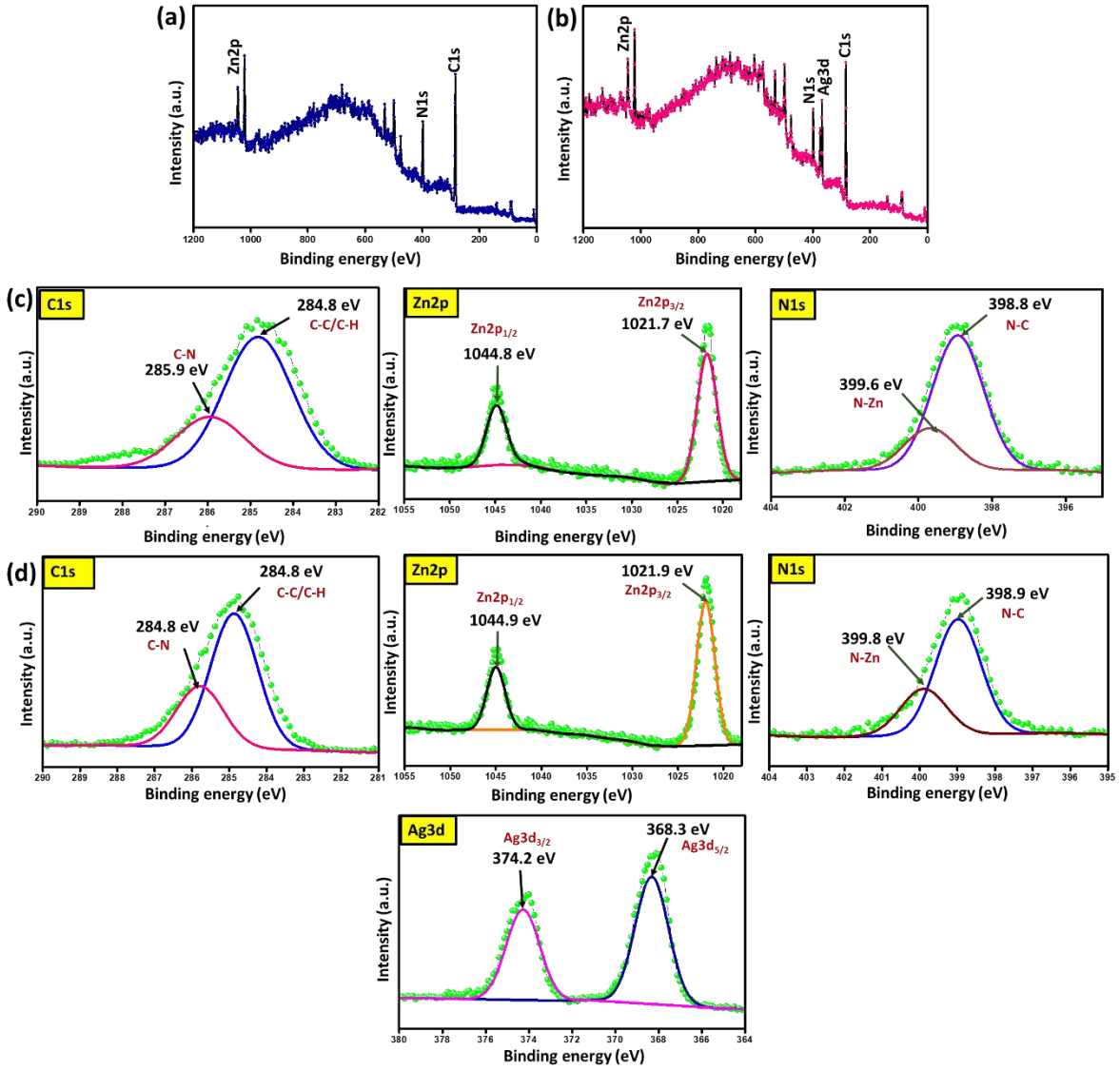


Figure 4: XPS survey spectra of (a) ZIF-8, (b) ZIF-8@Ag, high resolution deconvoluted spectra of (c) C1s, N1s and Zn2p of ZIF-8 and (d) C1s, N1s, Zn2p and Ag3d of ZIF-8@Ag

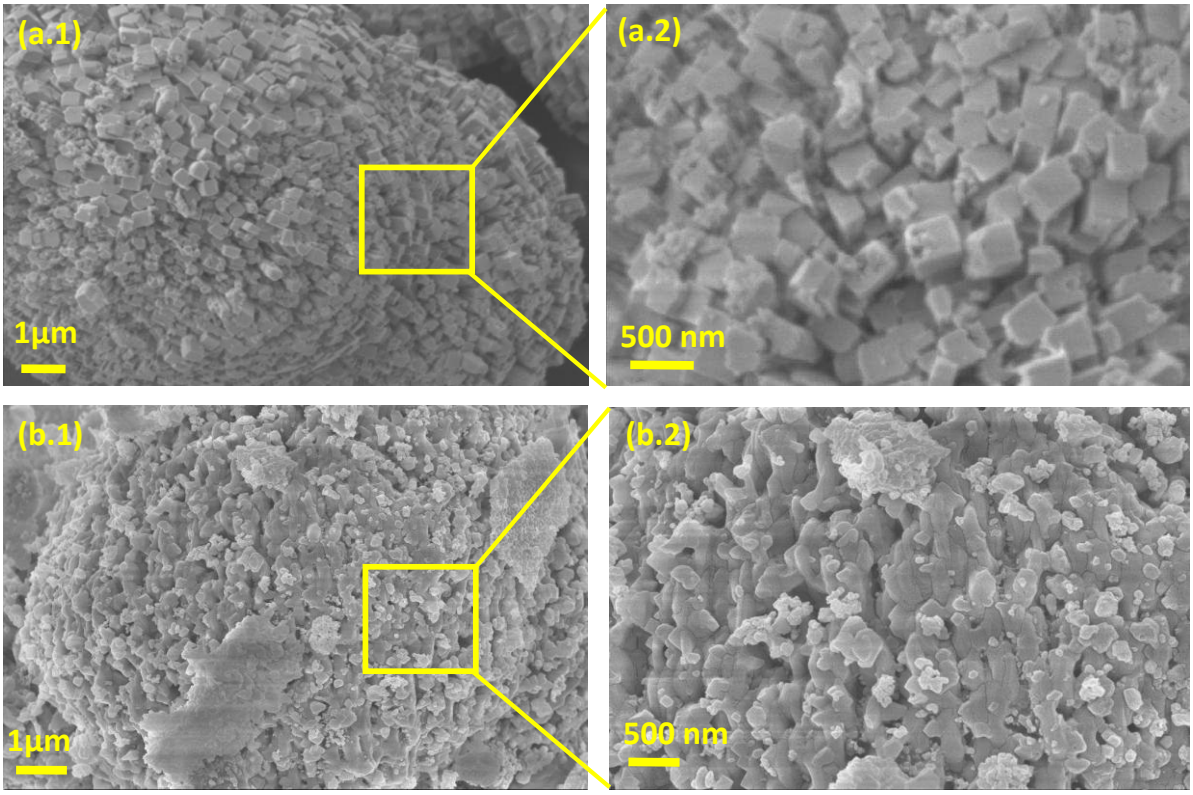


Figure 5: FESEM image of (a.1, a.2) ZIF-8 and (b.1, b.2) ZIF-8@Ag

3.2. Characterization of membranes

FTIR analysis of the fabricated membranes was done to get insights into the functional modifications carried out during membrane fabrication. M-0 membrane exhibits a broad peak at 3406 cm^{-1} which can be ascribed to N-H stretching vibration of NH_2 group present in PEGdiamine (Figure 6a.1). After ZIF-8@Ag incorporation, M-AZ membrane shows peak at 3440 cm^{-1} indicating N-H stretching (Figure 6a.2) (Rinawati et al. 2015). The peak intensity enhanced and broaden in M-AZCh (at 3428 cm^{-1}) and M-AZChA (at 3406 cm^{-1}) membranes due to the addition of chitosan which contains hydroxyl as well as amine functional groups. All four membranes exhibits common peaks at 2914 cm^{-1}, 1326 cm^{-1} and 617 cm^{-1} which represents of C-H stretching, CH_2 waggling/C-H deformation and C-Cl stretching vibration respectively (Ramesh and Arof 2001). C=C stretching of vinylidene group of PVC and N-H bending showed overlapping peaks in the range of 1600-1646 cm^{-1} in all the membranes (Rinawati et al. 2015). New peaks at 1028 cm^{-1} (in M-AZCh membrane) and at 1017 cm^{-1} (in M-AZChA membrane) have been observed which were originally absent in M-0 and M-AZ membranes. The occurrence of these new peaks arises after chitosan incorporation; they can be attributed to C-O stretching of primary alcohol present in chitosan. To investigate whether PEGdiamine remained in the M-0 membrane following water immersion during membrane fabrication, FTIR analysis of the M-0 and bare PVC membranes was carried out and

compared. FTIR spectra given in Figure S1 shows a N-H stretching characteristic peak around 3406 cm^{-1} in M-0 membrane, but the same is absent in pristine PVC membrane. Moreover, near 1600 cm^{-1}, peak orientation changes slightly indicating overlapping of C=C stretching of PVC and N-H bending of PEGdiamine.

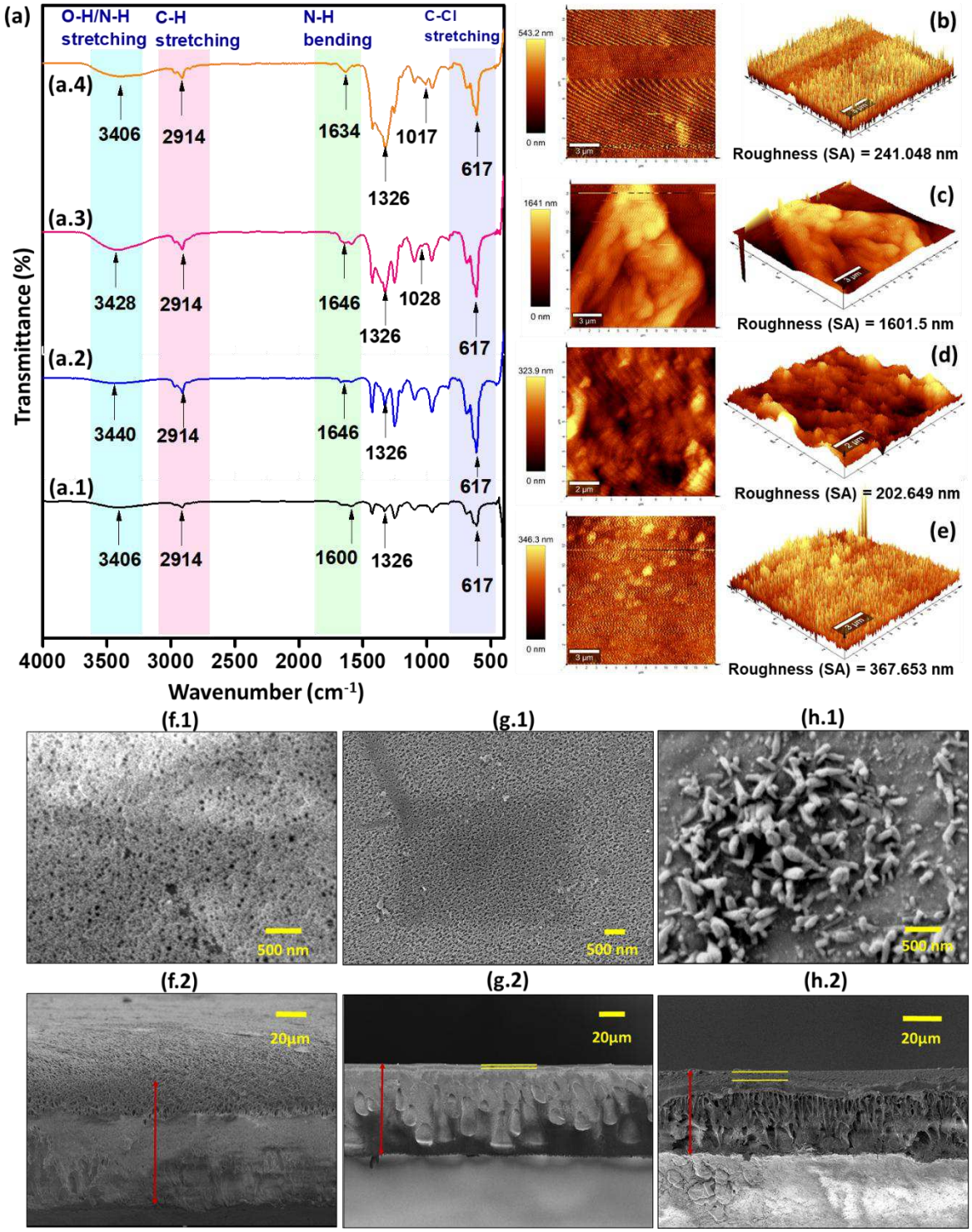


Figure 6: (a) FTIR spectra of different membranes (a.1) M-0, (a.2) M-AZ, (a.3) M-AZCh, (a.4) M-AZChA; AFM images of (b) M-0, (c) M-AZ, (d) M-AZCh and (e) M-AZChA membranes and their roughness value, (f.1, g.1,

h.1) FESEM surface images of M-0, M-AZ and M-AZCh membranes respectively; (f.2, g.2, h.2) FESEM cross-sectional image of M-0, M-AZ and M-AZCh membranes respectively

Surface roughness of the membranes was studied via AFM analysis and the obtained images are presented in Figure 6(b-e). The M-0 membrane exhibits surface roughness of 241.048 nm which increases to 630.076 nm after incorporation of ZIF-8@Ag in M-AZ membrane. After homogeneous coating of chitosan, obtained M-AZCh membrane experience a lowering in roughness value to 202.649 nm. However, treatment of membrane with Ag^+ introduces crosslinking with amine groups of chitosan, which enhances the roughness of the membrane to 367.653 nm.

FESEM analysis of the M-0, M-AZ and M-AZChA were done to analysis their surface as well as cross-sectional morphology. The surface image of M-0 membrane (Figure 6f.1) showed a porous, sponge like morphology. Cross-sectional image of M-0 membrane also validates this porous morphology (Figure 6f.2). However, the cross-section of M-0 membrane is appeared to be asymmetric containing both porous and dense portions. Partial removal of unbound PEGdiamine may be responsible for the spongy like porous structure. After ZIF-8@Ag incorporation, both the surface and cross-sectional morphology changes in M-AZ membrane. The surface as well as cross-section acquire uniform morphology and the pores are distributed uniformly throughout the matrix (Figure 6g.1 and 6g.2). The interaction of ZIF-8@Ag with the polymer's matrices may change the polymer chain packing, which generates the pores inside the membrane as evident from the cross-section (Figure 6g.2). In M-AZChA membrane, the surface clearly shows morphological change due to coating of chitosan and Ag^+ (Figure 6h.1, 6h.2). From cross-sectional image of M-AZChA membrane in Figure 6h.2, a porous inner structure with a dense outer layer is observed. The top dense layer can be attributed to the Ag^+ cross-linked chitosan structure.

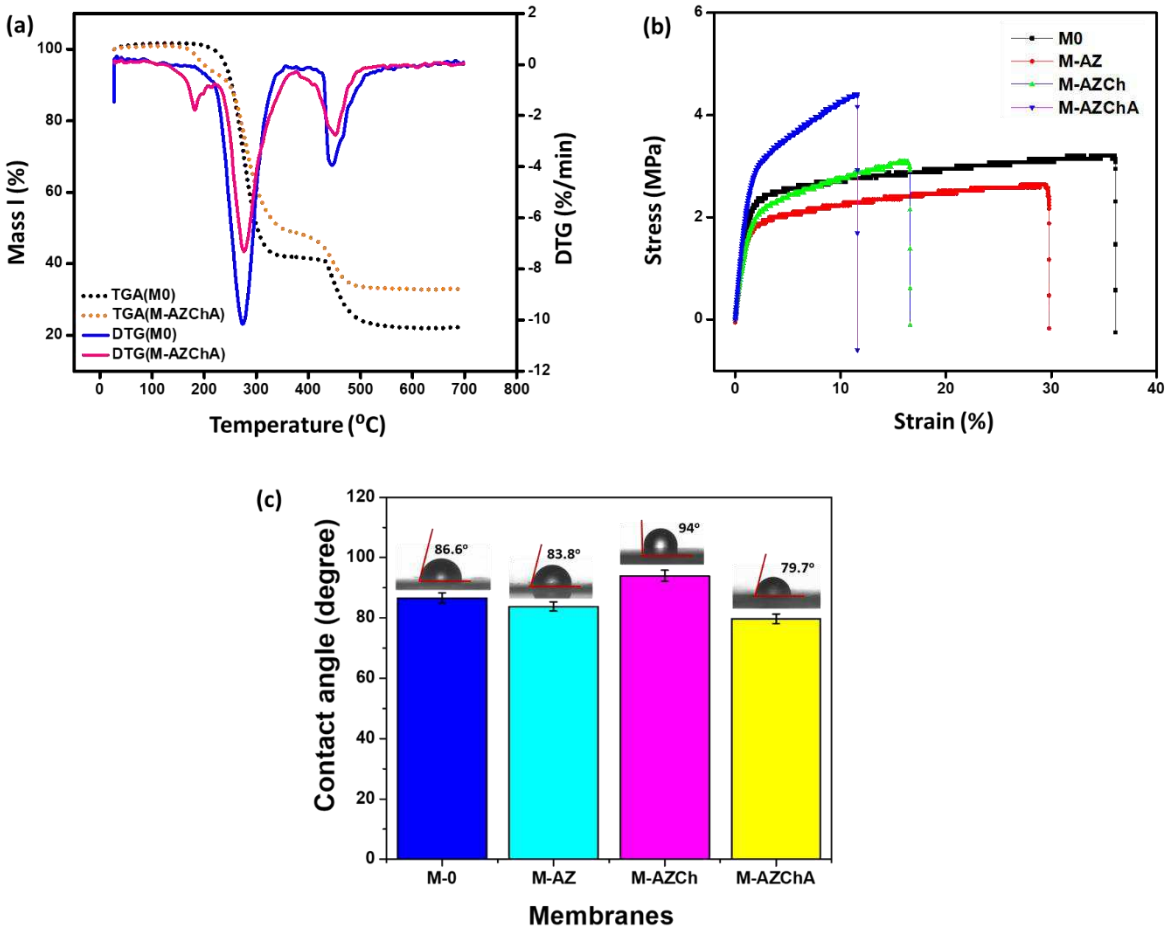


Figure 7: (a) TGA and DTG analysis of M-0 and M-AZChA membranes, (b) Stress vs strain graph and (c) contact angle analysis of the fabricated membranes

Thermogravimetric analysis (TGA) and differential thermogravimetric (DTG) analysis of the M-0 and M-AZChA membranes were conducted to check the membrane's thermal stability before and after modification (Figure 7a). M-0 membrane shows weight loss at two distinct stages at temperature 273 ºC and 447 ºC. The mass loss at 273 ºC can be attributed to dehydrochlorination of PVC leading to form polyene. The 2nd degradation at 447 ºC corresponds to molecular scission and polyene structure decomposition (Cruz et al. 2021). Similarly in M-AZChA membrane, PVC shows mass loss at 276 ºC and 449 ºC. The weight loss of PEGdiamine is also overlapped with the 2nd degradation of PVC at 447 ºC and 449 ºC of M-0 and M-AZChA membranes respectively. The shoulder obtained near 1st degradation peak of PVC at 276 ºC in M-AZChA membranes indicates the complex dehydrochlorination involving different events. Incorporation of chitosan in M-AZChA membrane may also exhibit mass loss of chitosan in the range of 200-300 ºC, however it appears to overlap with the existing degradation peak. Mechanical property analysis of the membranes suggests a visible change in stress and strain value upon various stages of modification (Figure 7b). M-0 membrane exhibits ultimate stress of 3.21 MPa, which

decreases to 2.64 MPa in M-AZ membrane after incorporation of ZIF-8@Ag in to the polymer matrix. Coating of chitosan boosts the ultimate stress value in M-AZCh membrane. Incorporation of Ag^+ facilitates cross-linking within chitosan layer, thereby increasing the overall mechanical strength to 4.41 MPa in M-AZChA membrane.

Contact angle measurements of the fabricated membranes provide valuable information regarding their surface wettability. (Figure 7c). Contact angle of M-0 membrane is 86.6º which indicates a moderately hydrophilic surface. Pure PVC membrane is well known for its hydrophobic nature, having water contact angle > 130º (Asmatulu et al. 2013). Modification of PVC with PEGdiamine significantly lower the water contact angle in M-0 membrane, which may be attributed to the amine groups and repetitive ethylene glycol group present in PEGdiamine. After ZIF-8@Ag incorporation, a slight decline in contact angle value is observed. This can relate to the high surface roughness of the membrane. In M-AZCh membrane contact angle value enhances to 94º which can be attributed to the hydrophobic backbone of chitosan chain (Almeida et al. 2010). Although chitosan has inherent hydrophilic groups such as -OH and $–NH_2$, there is a probability of structural rearrangement during temperature assisted drying of chitosan film. This rearrangement is mostly driven by the possible inter- and intra-molecular hydrogen bonding. As a result of the reorientation, functional groups able to form hydrogen bond become unavailable or less exposed on the membrane surface, which explains the high-water contact angle (94º) of M-AZCh membrane after chitosan layer coating (Hubbe 2019). After Ag^+ cross-linking, the surface roughness (Figure 6e) and polarity of the membrane are enhanced, which makes the membrane more hydrophilic, with a contact angle value of 79.7°.

XPS analysis of M-0 and M-AZChA membrane validate the successful modifications. XPS survey spectra of M-0 membrane show the presence of C1s, Cl2p, N1s and O1s peaks which are the key elements of PVC and PEGdiamine (Figure 8a). In M-AZChA membrane, in addition to C1s, Cl2p, N1s and O1s, additional peaks for Zn2p and Ag3d have been observed indicating the successful incorporation of ZIF-8@Ag (Figure 8b). C1s deconvolution spectra of M-0 membrane show binding environment of carbon. For C-C, C-N/C-Cl and C-O bindings, peaks at 284.8 eV, 285.8 eV and 286.8 eV have been obtained respectively (Figure 8c). O1s peaks at 532.3 eV represent O-C binding (Figure 8d). Representative peaks at 199.8 eV and 201.2 eV for $Cl2p_{3/2}$ and $Cl2p_{1/2}$ respectively have been observed in M-0 membrane (Figure 8e). N1s peaks at 397.9 eV and 399.6 eV indicate N-H and N-C bindings (Figure 8f). For M-AZChA membrane, C1s peaks arise at 284.7 eV, 285.4 eV, 285.8 eV and 287.2 eV which represents C-C, C-N, C-Cl and C-O bindings respectively (Figure 8g). O1s peaks at 531.1 eV, 532.2 eV and 533.1 eV correspond to C-O-C, O-C-O and O-H bindings respectively (Figure 8h). Cl2p shows the characteristics peaks for $2p_{3/2}$ and $2p_{1/2}$ (Figure 8i) whereas N1s shows peaks for N-H and N-C (Figure 8j). From Figure 8k, characteristic peaks of Ag3d at 367.6 eV ($3d_{5/2}$) and 373.6 eV ($3d_{3/2}$) are observed. Similarly, Zn2p

deconvolution shows characteristic peaks at 1021.9 eV and 1045 eV, corresponds to $Zn2p_{3/2}$ and $Zn2p_{1/2}$ respectively (Figure 8l).

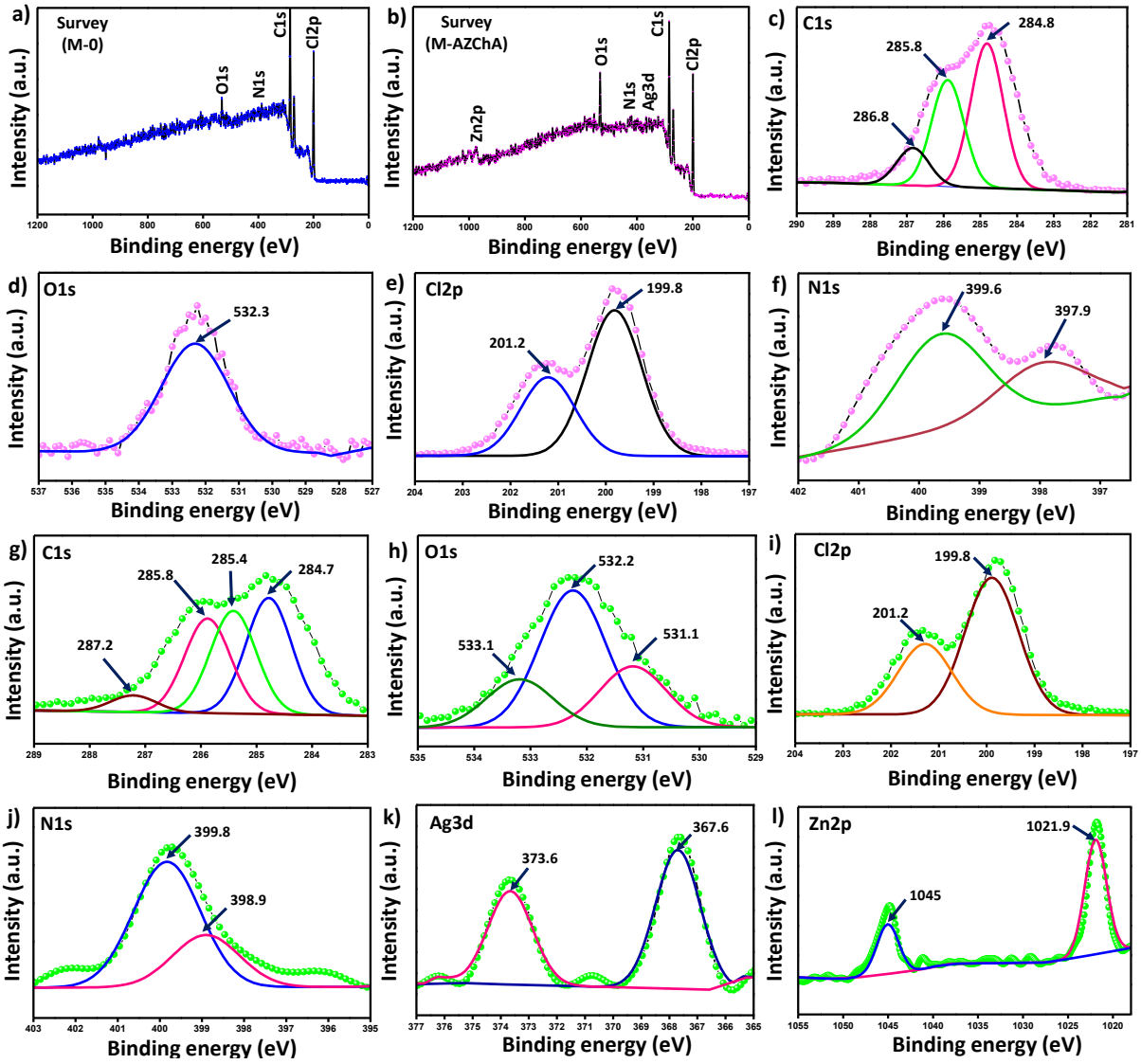


Figure 8: XPS survey of (a) M-0 and (b) M-AZChA membrane; high resolution elemental deconvolution of (c-f) M-0 and (g-l) M-AZChA membrane

N_2 adsorption desorption isotherm of M-AZ and M-AZChA membranes presented in Figure S2(a) and S2(b) respectively shows Type-IV hysteresis loops which indicates the mesoporous nature of the membranes (pore range in 2-50 nm). However, a decrease in volume of N_2 uptake has been observed in M-AZChA membrane. Pore size distribution of M-AZ and M-AZChA membranes has been analysed and provided in Figure S2(c) and S2 (d) respectively. The most of the pores in M-AZ membrane have pore radius of 15.7. After surface modification with chitosan/Ag^+, the pore size becomes smaller and most of the pores in M-AZChA membrane have radius of 13.8 Å.

3.3. Gas transport and separation study

The permeance of the pure gases H_2, N_2, O_2, C_2H_6 and C_2H_4 are measured for all the fabricated membranes at room temperature. As PVC is known as a glassy polymer and reportedly exhibited low gas permeability (Tiemblo et al. 2002). Herein, the PVC membrane after nanofiller (ZIF-8@Ag) incorporation exhibit high gas permeances for the experimented gases. M-AZ membrane exhibited highest H_2 permeance of 6258 GPU, N_2 permeance of 2374 GPU and O_2 permeance of 2265 GPU (Figure 9a). The membrane also showed almost same permeance for C_2H_4 and C_2H_6. The enhanced gas permeance can be attributed to the generation of free volume inside membrane matrix upon nanofiller and PEGdiamine incorporation, which can influence the polymer chain packing and can alter the overall performance of the membrane. The selectivity of gas pairs: H_2/N_2, O_2/N_2 and C_2H_4/C_2H_6 have been measured using Equation 2 and presented in Figure 9b. M-AZ membrane exhibited a moderate selectivity of 2.6 for H_2/N_2. The same membrane demonstrated O_2/N_2 and C_2H_4/C_2H_6 selectivity of 0.95 and 1 respectively. The resultant selectivity is well aligned with ideal Knudsen diffusion selectivity which is often observed in porous membranes. To study the impact of additionally coated chitosan layer on membrane performance, permeance and selectivity of gases through M-AZCh membrane has been studied. M-AZCh membrane consists of chitosan layer over a ZIF-8@Ag incorporated MMMs as membrane support. The chitosan layer reduced the gas permeance of all the gases, with H_2 exhibiting highest permeance of 298 GPU. This reduction can be explained from the transport resistance induced by the chitosan layer. The layer of chitosan increases the path of gas diffusion and also restricts the gas transport through the membrane. As a result, decrease in gas selectivity of the M-AZCh membrane has also been witnessed. Cross-linking of chitosan with Ag^+ produces M-AZChA membrane. The chitosan/Ag^+ layer of M-AZChA membrane is thicker and denser, as evident from FESEM analysis (Figure 6h.2). Lowering of gas permeance for all the gases are witnessed in M-AZChA membrane which can be ascribed to the thick nature of the membrane selective layer. After incorporation of Ag^+ in chitosan matrix, a slight improvement in H_2/N_2 and O_2/N_2 selectivity are observed (Figure 9b). Incorporation of Ag^+ in chitosan promotes interactions with $–NH_2$ and –OH functional groups, which results in a physically cross-linked compact structure, which may explain the increase in selectivity at the expense of permeance.

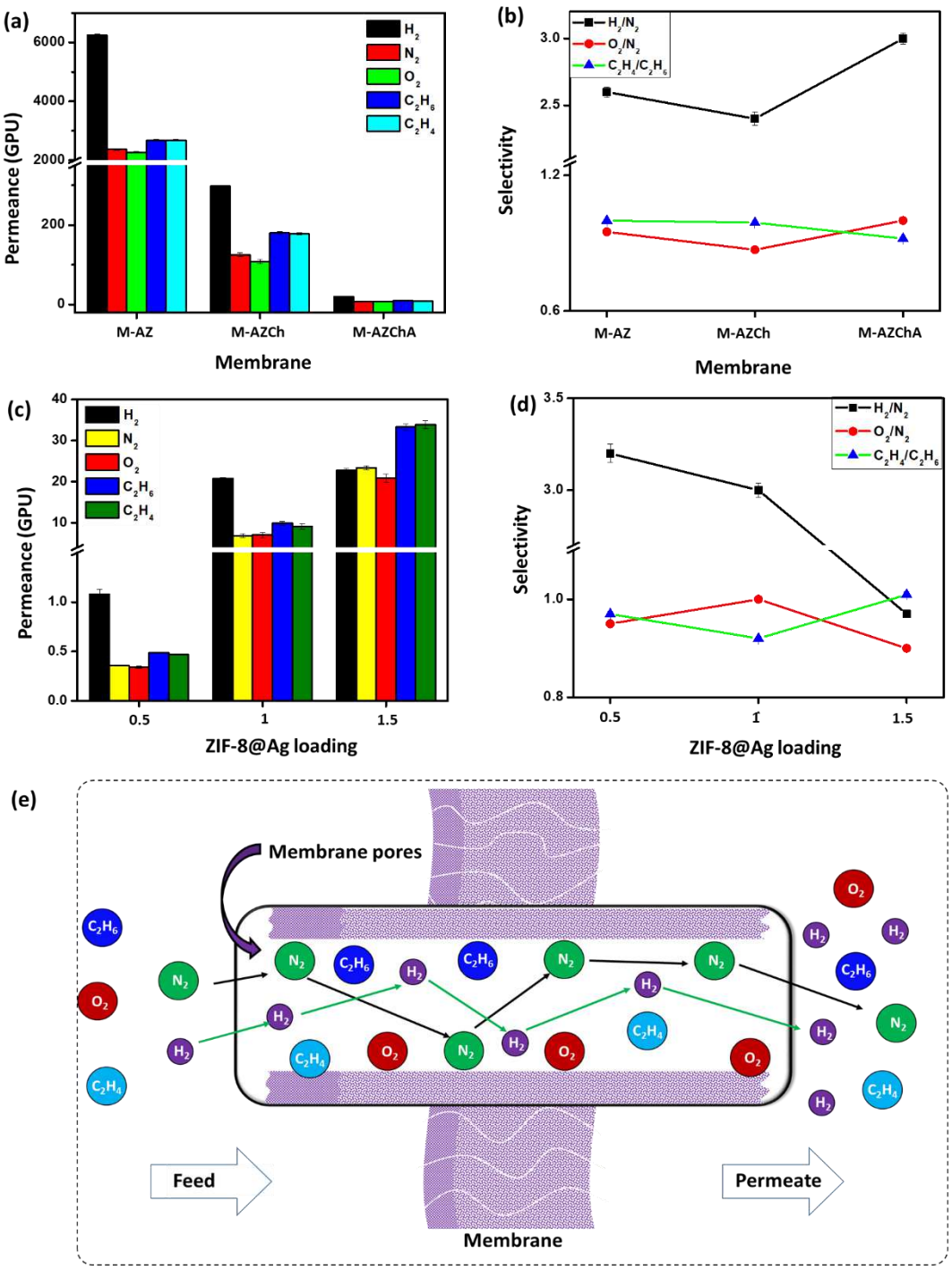


Figure 9: (a) Gas permeance and (b) selectivity of M-AZ, M-AZCh and M-AZChA(1 wt.% AZ loading) membranes, (c) Gas permeance and (d) selectivity of M-AZChA membrane at different AZ loading (0.5 wt.%, 1 wt.%, 1.5 wt.%), (e) Knudsen diffusion controlled gas transport through the membrane pores

To elucidate the impact of ZIF-8@Ag loading on membrane performance, the concentration is varied as 0.5, 1 and 1.5 wt. % in M-AZChA membrane (Figure 9c and 9d). At 0.5 wt. % ZIF-8@Ag loading, the gas permeance are very low. However, slight increase in H_2/N_2 selectivity of 3.2 has been witnessed. At 1 wt. % ZIF-8@Ag

loading, gas permeance enhances with H_2/N_2 selectivity of 3. At 1.5 wt. % loading, further enhancement in gas permeance are observed at the expense of selectivity. The results indicate that increasing ZIF-8@Ag loading boosts gas transport property of the membranes; however, this improvement is accompanied by a decline in H_2/N_2 selectivity. Increase in ZIF-8@Ag concentration affect the membrane inner structure and may introduce free volumes it, which may be the reason behind the enhancement of gas permeance and lowering of selectivity.

3.4. Plausible mechanism

The gas transport mechanism through the membranes may vary depending on various factors: membrane materials, pore structure and most importantly properties of the gas molecules. The M-AZChA membrane exhibits a selective layer and provides low gas permeance along with H_2/N_2 selectivity lies near 3 whereas the same for O_2/N_2 and C_2H_4/C_2H_6 are ~1. These exhibited selectivity values are very close to the theoretical Knudsen selectivity, indicating Knudsen diffusion to be followed predominantly by the gas molecules under the investigated conditions. This behaviour may be attributed to be intrinsic low solubility of the target gases/gas pairs in the polymer matrix. Gases such as H_2, N_2 and O_2 are less condensable in nature providing less possibility of solubility-based transport. Thus, despite the presence of dense layer, no significant discrimination is obtained during the transport of the target gases, leading to a low selectivity, which approaches theoretical Knudsen selectivity. Knudsen diffusion is pre-dominant in membranes when the size of pore approaches the mean free path of the scattered gas molecule (Akilu et al. 2021). The mean free path of H_2 is greater than the pore size of the membrane in the applied pressure range. It suggests that H_2 follows Knudsen diffusion dominantly during transportation. In case of other gases viz. N_2, O_2, C_2H_4 and C_2H_6, mean free path are greater than the pore diameter of the membrane, which indicates the dominance of Knudsen diffusion during their transport through the membrane. The molecular weight of gas also plays crucial role while differentiating their diffusion rate to measure ideal Knudsen selectivity. The molecular weight of the gases is inversely proportional to the diffusion rate. Theoretically, H_2 diffuses about 3.74 times faster than N_2 if the transport is governed purely by Knudsen diffusion. Experimentally observed selectivity by the fabricated membranes are ~ 3 which is consistent with a Knudsen-dominated mechanism. In case of O_2/N_2 and C_2H_4/C_2H_6 also, the observed selectivity is aligned with the Knudsen selectivity. The aim behind silver ion incorporation is to facilitate the transport of C_2H_4 over C_2H_6 via π-complexation interactions. However, no significant enhancement in selectivity has been observed to refer the mechanism as facilitated transport. This may be explained from the unavailability of silver in active Ag(I) state due to its participation in cross-linking, which thereby limits its participation as carrier in facilitated transport. As an overall observation, various gas transports through the fabricated membranes were found to be predominantly controlled by Knudsen diffusion (Figure 9e).

3.5. Comparison with literature

Table S3 and S4 of the Supplementary Materials present the key results obtained in the present study alongside related literature data, enabling a comparative evaluation of the performance of the membrane. The M-AZ membrane showed higher gas permeability than most of the membranes reported in literature. The gas permeability of M-AZCh membrane was nearly comparable with the literature, whereas M-AZChA membrane displayed relatively lower permeability. In case of selectivity, all the fabricated membranes underperformed compared to the literature data. The lower selectivity can be explained from the porous nature of the membrane which promoted the transport of gases predominantly via Knudsen diffusion mechanism rather than molecular sieving or facilitated transport.

3.6. Dye separation study

The designed membrane's applicability in water treatment was also evaluated for analyse the membrane's capability for removal of organic contaminants from water/wastewater. For this dye separation experiment was conducted with 50 ppm MB dye aqueous solution as the feed. Using a stirred membrane cell (shown in Figure S4 of the Supplementary Materials) the water flux and dye removal efficiency of the membranes are studied at a feed pressure of 2 bar and ambient temperature. The water flux of M-0 and M-AZ membranes are provided in Figure 10a. The flux data clearly showed that M-AZ membrane showed high flux than M-0 membrane. The highest flux provided by M-AZ membrane is 58.2 $L.m^{-2}.h^{-1}$. It can be explained from the ZIF-8/Ag incorporation in the membrane matrix, which enhances the internal free volume of the membrane by creating additional water transport pathway. The intrinsic cage like porous structure of ZIF-8/Ag as well as disruption of polymer packing upon ZIF-8@Ag incorporation are the main reason behind the free volume enhancement inside the membrane, which leads to increase in the water flux value. However, in M-AZCh and M-AZChA membranes, no water permeability can be observed at the same operating condition, which is due to the dense chitosan and Ag^{+} crosslinked chitosan layer respectively. The absorption spectra of feed (dye) and permeate of M-0 and M-AZ membranes showed a significant reduction in peak intensity evidencing the rejection attained by the membranes (Figure 10b). The rejection efficiency of M-AZ membrane is found to be higher than the M-0 membrane (Figure 10c). A highest MB rejection of 69.7% have been obtained by the M-AZ MMMs. The rejection % of the membranes tends to increase slightly with time which can be attributed to the filling up of the adsorption sites and pores of the membranes by dye molecules. This increment in rejection % is not significant as the stir bar placed inside the membrane cell can cause turbulence in water which eventually prevent the cake layer formation on membrane surface. The rejection % in M-AZ membrane can be attributed to the interaction possibility between ZIF-8@Ag and MB dye. As represented in Figure 10d, both coordination interaction and π-π interaction may take place between MB and ZIF-8@Ag which

explain the rejection behaviour. Ag have the ability to adsorb MB dye via coordination interaction, which contribute towards the improved dye rejection exhibited by the membrane (Zhong et al. 2010). Moreover, MB molecule is regarded to have an approximate rectangular volume of dimensions 17 × 7.6 × 3.3 Å (Arias et al. 1999). The membrane M-AZ have maximum pores in the diameter of 31.4 Å (radius = 15.7 Å). Thus, a sieving based separation of dye may also take place simultaneous to the adsorption process.

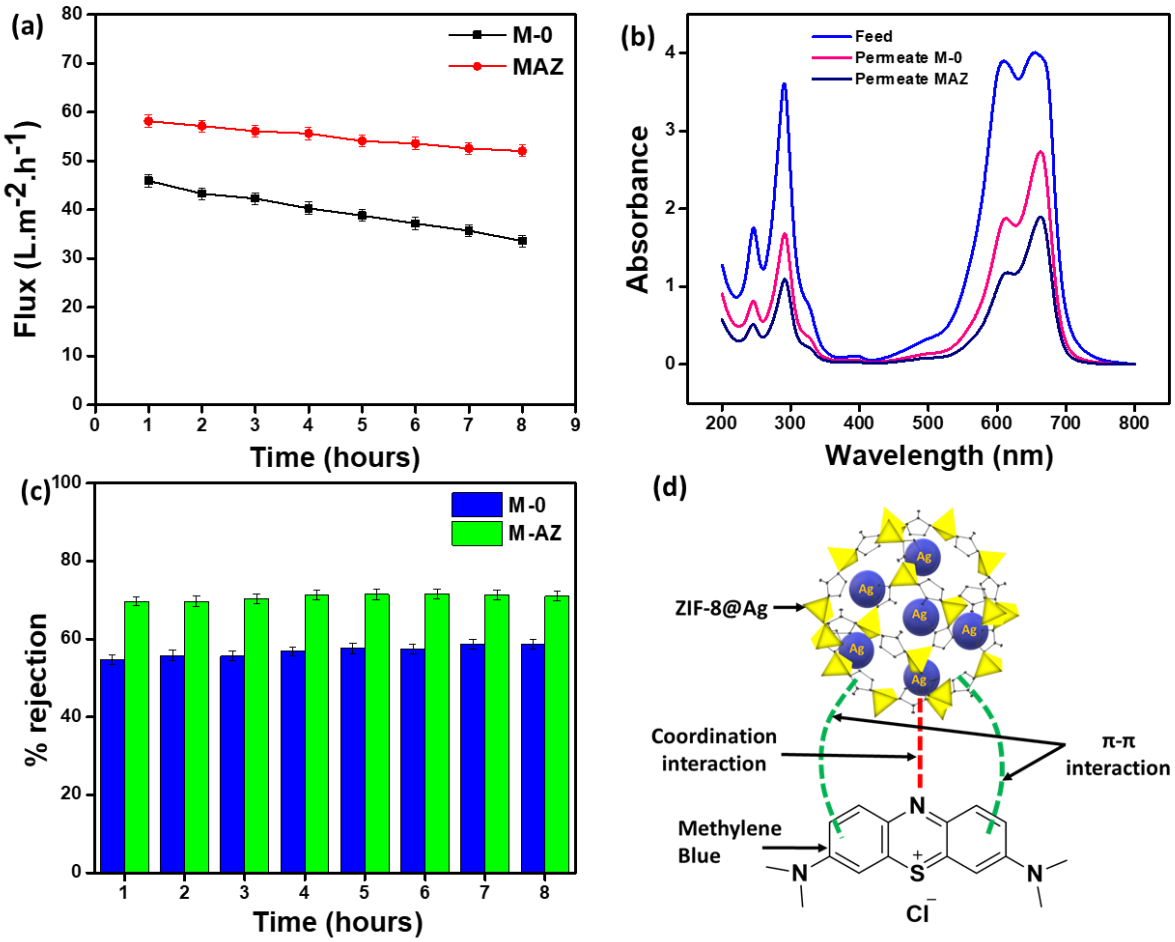


Figure 10: (a) Flux of M-0 and M-AZ membrane, (b) UV-Vis absorption spectra of feed and permeates, (c) rejection % of MB dye by M-0 and M-AZ membrane, (d) plausible interaction between MB dye and ZIF-8@Ag

4. Conclusion

This study has demonstrated the successful synthesis of ZIF-8 and ZIF-8@Ag. ZIF-8@Ag incorporated PVC/PEGdiamine MMMs have been implemented in gas transport study of varied gases (H_2, N_2, O_2, C_2H_4 and C_2H_6). The MMM exhibit highest H_2 permeance of 6258 GPU. Effect of chitosan and Ag^+ cross-linked chitosan layer on the gas transport behaviour of the membranes have been analysed. Ag^+ cross-linked chitosan coated membrane (M-AZChA) showed highest selectivity of 3.2 at 0.5 wt. % ZIF-8@Ag loading with low H_2 permeance of 1.08 GPU. The same membrane exhibits selectivity of 3 at 1 wt. % ZIF-8@Ag loading with H_2 permeance of

20.8 GPU. An increasing trend in gas permeance is witnessed in M-AZChA membrane with increase in ZIF-8@Ag content. The overall mechanism act dominantly during the gas transport is predicted to be Knudsen diffusion. In conclusion, while some of the membranes demonstrated excellent gas permeance, careful structural and compositional modifications are still necessary to achieve improved selectivity. Subsequent evaluation of membrane performance in water treatment is also done. The M-AZ membrane demonstrated an appreciable water flux of 58.2 $L.m^{-2}.h^{-1}$ along with MB dye removal efficiency of 69.7 to 71%. This results suggest that the membrane possesses great potential for multifunctional applications, extending beyond gas separation to water treatment. The key novelty lies in the overall membrane structure and dual functionality of the membrane in both gas and water treatment. Unlike other, the membrane fabricated in the current study demonstrates versatility. Though the separation performance obtained are moderate, the concept of dual functional membrane synthesis can provide a base for future research to enable efficient resource utilization, cross-sector applicability and sustainability.

Among the synthesized membranes, M-AZ MMMs provides good combination of gas perm-selectivity and dye rejection efficiency. Synthesis of this membrane involves simple blending of polymer and filler material at relatively low temperature (< 80 ºC) and atmospheric pressure. However total dissolution and mixing time to prepare dope solution is slightly higher for its commercial scale production. Future research could consider optimizing the dope solution preparation time via process intensification or continuous flow synthesis to enhance industrial or commercial viability.

Supplementary Materials

FTIR spectra of bare PVC and PVC-PEGdiamine (M-0) membrane (Figure S1), N_2 adsorption desorption isotherm and Pore size distribution analysis of (Figure S2) membrane, Experimental condition of gas permeation Test (Table S1), EDX analysis of ZIF-8@Ag (Figure S3 and Table S2), Comparison table of current study with literature (Table S3 and S4), Dye separation set-up (Figure S4)

REFERENCES

Abdi J (2020) Synthesis of Ag-doped ZIF-8 photocatalyst with excellent performance for dye degradation and antibacterial activity. Colloids Surf A Physicochem Eng Asp 604:125330. https://doi.org/10.1016/j.colsurfa.2020.125330

Adams RT, Lee JS, Bae TH, Ward JK, Johnson JR, Jones CW, Nair S, Koros WJ (2011) CO_2–CH_4 permeation in high zeolite 4A loading mixed matrix membranes. J Membr Sci 367:197–203. https://doi.org/10.1016/j.memsci.2010.10.059

Ahmadpour E, Shamsabadi AA, Behbahani RM, Aghajani M, Kargari A (2014) Study of CO_2 separation with PVC/Pebax composite membrane. J Nat Gas Sci Eng 21:518–523. https://doi.org/10.1016/j.jngse.2014.09.021

Akilu S, Padmanabhan E, Sun Z (2021) A review of transport mechanisms and models for unconventional tight shale gas reservoir systems. Int J Heat Mass Transf 175:121125. https://doi.org/10.1016/j.ijheatmasstransfer.2021.121125

Almeida EVR, Frollini E, Castellan A, Coma V (2010) Chitosan, sisal cellulose, and biocomposite chitosan/sisal cellulose films prepared from thiourea/NaOH aqueous solution. Carbohydr Polym 80:655–664. https://doi.org/10.1016/j.carbpol.2009.10.039

Alomar M, Shahzadi K, Alotaibi A, Sarfraz M (2026a) Decarbonization via polyethersulfone-based composite membranes containing bimetallic Zn-Co nanoferrites. Surf Interfaces. https://doi.org/10.1016/j.surfin.2026.108628

Alomar M, Sharif S, Albarzan B, Alotaibi A, Sarfraz M (2026b) Water purification via interfacially polymerized thin film composite membranes. Polym Int 75:631–642. https://doi.org/10.1002/pi.70091

Ameer AA, Abdallh MS, Ahmed AA, Yousif EAS (2013) Synthesis and characterization of polyvinyl chloride chemically modified by amines. Open J Polym Chem 3:11–15. https://doi.org/10.4236/ojpchem.2013.31003

Arias M, López E, Nuñez A, Rubinos D, Soto B, Barral MT, Díaz-Fierros F (1999) Adsorption of methylene blue by red mud, an oxide-rich byproduct of bauxite refining. In: Effect of mineral-organic-microorganism interactions on soil and freshwater environments. Springer, Boston, MA, pp 361–365. https://doi.org/10.1007/978-1-4615-4683-2_39

Asmatulu R, Muppalla H, Veisi Z, Khan WS, Asaduzzaman A, Nuraje N (2013) Study of hydrophilic electrospun nanofiber membranes for filtration of micro and nanosize suspended particles. Membranes 3:375–388. https://doi.org/10.3390/membranes3040375

Barjasteh M, Dehnavi SM, Ahmadi Seyedkhani S, Rahnamaee SY, Golizadeh M (2023) Synergistic wound healing by novel Ag@ZIF-8 nanostructures. Int J Pharm 630:122339. https://doi.org/10.1016/j.ijpharm.2022.122339

Basu S, Cano-Odena A, Vankelecom IFJ (2011) MOF-containing mixed-matrix membranes for CO_2/CH_4 and CO_2/N_2 binary gas mixture separations. Sep Purif Technol 81:31–40. https://doi.org/10.1016/j.seppur.2011.06.037

Bhuyan C, Bora P, Rajguru P, Hazarika S (2025) Thin film nanocomposite membrane ornamented with Z-scheme heterojunction carbon dot/NiFe–LDH for removal of organic contaminants from industrial wastewater. Sep Purif Technol 356:129791. https://doi.org/10.1016/j.seppur.2024.129791

Bora P, Bhuyan C, Borah AR, Hazarika S (2023) Carbon nanomaterials for designing next-generation membranes and their emerging applications. Chem Commun 59:11320–11336. https://doi.org/10.1039/D3CC02535H

Bora P, Bhuyan C, Hazarika S (2026) Chitosan carbon dot cross-linked layered double hydroxide-coated high-performance thin-film nanocomposite membranes for facile CO_2 separation. ACS Appl Eng Mater 4:866–881. https://doi.org/10.1021/acsaenm.5c01046

Bora P, Bhuyan C, Rajguru P, Hazarika S (2023) A Gemini basic ionic liquid and functionalized cellulose nanocrystal-based mixed matrix membrane for CO_2/N_2 separation. Chem Commun 59:12887–12890. https://doi.org/10.1039/D3CC03628F

Chen J, Gao Q, Zhang X, Liu Y, Wang P, Jiao Y, Yang Y (2019) Nanometer mixed-valence silver oxide enhancing adsorption of ZIF-8 for removal of iodide in solution. Sci Total Environ 646:634–644. https://doi.org/10.1016/j.scitotenv.2018.07.298

Cruz PPR, da Silva LC, Fiuza-Jr RA, Polli H (2021) Thermal dehydrochlorination of pure PVC polymer: Part I—thermal degradation kinetics by thermogravimetric analysis. J Appl Polym Sci 138:50598. https://doi.org/10.1002/app.50598

Dilshad MR, Islam A, Haider B, Sajid M, Ijaz A, Khan RU, Khan WG (2021) Effect of silica nanoparticles on carbon dioxide separation performances of PVA/PEG cross-linked membranes. Chem Pap 75:3131–3153. https://doi.org/10.1007/s11696-020-01486-7

El-Sawaf A, Ahmed S, Nassar A, Mubarak M (2024) Synergistic breakthroughs in seawater desalination: zirconium-based MOF/PVC-PVA composite membranes for unprecedented performance. Res Square. https://doi.org/10.21203/rs.3.rs-4193187/v1

Geng Y, Xu J, Wu Q, Liu Y, Wu Y, Liu K, Wang D (2024) Nanoparticle-filled oriented nanofiber membrane for effective emulsion separation via spin coating. Compos Commun 48:101939. https://doi.org/10.1016/j.coco.2024.101939

Hashem MAH (2023) Electrospun PVC/MOFs-Ag nanocomposites as efficient antibacterial membranes. Doctoral dissertation. https://hdl.handle.net/10938/23861

Hashem MH, Wehbe M, Damacet P, El Habbal RK, Ghaddar N, Ghali K, Ahmad MN, Karam P, Hmadeh M (2023) Electrospun metal–organic framework-fabric nanocomposites as efficient bactericides. Langmuir 39:9503. https://doi.org/10.1021/acs.langmuir.3c01039

He J, Qu W, Feng Y, Jiang J, Luo J, Wu Y, Peng L (2024) Multiple synergistic antibacterial melamine-impregnated paper based on nano Ag-doped ZIF-8. Chem Eng J 493:152453. https://doi.org/10.1016/j.cej.2024.152453

Hubbe MA (2019) Why, after all, are chitosan films hydrophobic? BioResources 14:7630–7631. https://doi.org/10.15376/biores.14.4.7630-7631

Ismail AF, Rahim NH, Mustafa A, Matsuura T, Ng BC, Abdullah S, Hashemifard SA (2011) Gas separation performance of polyethersulfone/multi-walled carbon nanotubes mixed matrix membranes. Sep Purif Technol 80:20–31. https://doi.org/10.1016/j.seppur.2011.03.031

Ji Y, Wang Y, Liu Y, Luo J, Bai M, Chen L, Ling H, Zong X, Xue S (2026) Using maleimide-induced dual cross-linking method to fabricate high-performance mixed matrix membrane. ACS Appl Mater Interfaces 18:25142–25153. https://doi.org/10.1021/acsami.5c20217

Jiao C, Li Z, Li X, Wu M, Jiang H (2021) Improved CO_2/N_2 separation performance of Pebax composite membrane containing polyethyleneimine functionalized ZIF-8. Sep Purif Technol 259:118190. https://doi.org/10.1016/j.seppur.2020.118190

Jo JH, Lee CO, Ryu GY, Jae H, Roh D, Chi WS (2022) Hierarchical amine-functionalized ZIF-8 mixed-matrix membranes with an engineered interface and transport pathway for efficient gas separation. ACS Appl Polym Mater 4:6426–6439. https://doi.org/10.1021/acsapm.2c00843

Katare A, Sharma S, Horo H, Bhowmick S, Kundu LM, Mandal B (2023) An investigation on the effects of both amine grafting and blending with biodegradable chitosan membrane for CO_2 capture from CO_2/N_2 gas mixtures. Chem Eng J 466:143215. https://doi.org/10.1016/j.cej.2023.143215

Khajavian M, Salehi E, Vatanpour V (2020) Nanofiltration of dye solution using chitosan/poly(vinyl alcohol)/ZIF-8 thin film composite adsorptive membranes with PVDF membrane beneath as support. Carbohydr Polym 247:116693. https://doi.org/10.1016/j.carbpol.2020.116693

Khalilinejad I, Sanaeepur H, Kargari A (2015) Preparation of poly(ether-6-block amide)/PVC thin film composite membrane for CO_2 separation: effect of top layer thickness and operating parameters. J Membr Sci Res 1:124–129. https://doi.org/10.22079/jmsr.2015.14483

Khan HAA, Ramzan N, Alomar M, Sarfraz M (2026) Decarbonization via composite membranes synergistically impregnated with ZIF-67 and CNTs nanofillers. Polym Bull 83:302. https://doi.org/10.1007/s00289-026-06364-y

Li QQ, Li Y, Mao H, Zhang YM, Zhang QY, Chen XR, Zhao ZP (2025) Bimetallic engineering in Ag/Zn-ZIF-8/Pebax mixed matrix membranes for enhanced CO_2 separation. J Membr Sci:125046. https://doi.org/10.1016/j.memsci.2025.125046

Liu G, Li L, Huang X, Zheng S, Xu X, Liu Z, Zhang Y, Wang J, Lin H, Xu D (2018) Adsorption and removal of organophosphorus pesticides from environmental water and soil samples by using magnetic multi-walled carbon nanotubes@organic framework ZIF-8. J Mater Sci 53:10772–10783. https://doi.org/10.1007/s10853-018-2352-y

Liu Y, Zhao S, Xu C, Huang J, Guo Z (2025) Construction of ZIF-8 composited hydrogel coated PVDF membrane with durable superhydrophilicity and dyes adsorption properties for efficient separation of emulsified and dyed wastewater. Sep Purif Technol 353:128299. https://doi.org/10.1016/j.seppur.2024.128299

Min SB, Kang M, Han YJ, An I, Park BR, Kim JH, Kim JH (2024) Chitosan/Ag(I) thin-film composite membranes with high CO/N_2 separation performance by facilitated transport: effect of preparation and operation conditions. Sep Purif Technol 328:124931. https://doi.org/10.1016/j.seppur.2023.124931

Niu Y, Chen Y, Bao S, Sun H, Wang Y, Ge B, Li P, Hou Y (2022) Fabrication of polyarylate thin-film nanocomposite membrane based on graphene quantum dots interlayer for enhanced gas separation performance. Sep Purif Technol 293:121035. https://doi.org/10.1016/j.seppur.2022.121035

Niu Z, He N, Yao Y, Ma A, Zhang E, Cheng L, Li Y, Lu X (2024) Mixed matrix membranes for gas separations: a review. Chem Eng J 494:152912. https://doi.org/10.1016/j.cej.2024.152912

Noorani N, Mehrdad A (2019) Adsorption, permeation, and DFT studies of PVC/PVIm blends for separation of CO_2/CH_4. J Mol Liq 292:111410. https://doi.org/10.1016/j.molliq.2019.111410

Noorani N, Mehrdad A (2020) Modification of PVC with 1-vinylimidazole for CO_2/CH_4 separation: sorption, permeation and DFT studies. Phys Chem Res 8:689–703. https://doi.org/10.22036/pcr.2020.227164.1757

Papurello RL, Lozano LA, Ramos-Fernández EV, Fernández JL, Zamaro JM (2019) Post-synthetic modification of ZIF-8 crystals and films through UV light photoirradiation: impact on the physicochemical behavior of the MOF. ChemPhysChem 20:3201–3209. https://doi.org/10.1002/cphc.201900863

Parashar PK, Komarala VK (2017) Engineered optical properties of silver-aluminum alloy nanoparticles embedded in SiON matrix for maximizing light confinement in plasmonic silicon solar cells. Sci Rep 7:12520. https://doi.org/10.1038/s41598-017-12826-1

Park KS, Ni Z, Côté AP, Choi JY, Huang R, Uribe-Romo FJ, Chae HK, O'Keeffe M, Yaghi OM (2006) Exceptional chemical and thermal stability of zeolitic imidazolate frameworks. Proc Natl Acad Sci USA 103:10186–10191. https://doi.org/10.1073/pnas.0602439103

Patil M, Hunasikai SG, Mathad SN, Patil AY, Hegde CG, Sudeept MA, Amshumali MK, Elgorban AM, Wang S, Wong LS, Syed A (2023) Enhanced O_2/N_2 separation by quaternized Matrimid/multiwalled carbon nanotube mixed-matrix membrane. Heliyon 9:e21992. https://doi.org/10.1016/j.heliyon.2023.e21992

Peng D, Feng X, Yang G, Niu X, Liu Z, Zhang Y (2023) In-situ growth of silver complex on ZIF-8 towards mixed matrix membranes for propylene/propane separation. J Membr Sci 668:121267. https://doi.org/10.1016/j.memsci.2022.121267

Ramesh S, Arof AK (2001) Structural, thermal and electrochemical cell characteristics of poly(vinyl chloride)-based polymer electrolytes. J Power Sources 99:41–47. https://doi.org/10.1016/S0378-7753(00)00690-X

Ravinayagam V, Rehman S (2020) Zeolitic imidazolate framework-8 (ZIF-8) doped TiZSM-5 and mesoporous carbon for antibacterial characterization. Saudi J Biol Sci 27:1726–1736. https://doi.org/10.1016/j.sjbs.2020.05.016

Rinawati L, Nugraha RE, Munifa RMI, Chasanah U, Wahyuningsih S, Ramelan AH (2015) Increasing the effectiveness of pesticides based urea nanofertilizer encapsulated nanosilica with addition of rice husk TiO_2 additive substances. J Chem Pharm Res 7:85–89.

Rodriguez R, Palma MS, Bhandari D, Tian F (2023) Electrodeposition of Ag/ZIF-8-modified membrane for water remediation. Langmuir 39:2291–2300. https://doi.org/10.1021/acs.langmuir.2c02947

Shan Y, He M, Zhang F, Wang Y, Liu Y, Yang Y, Wang X, Zhang X, Li Y, Wang Z, Chen X (2023) Plasma-assisted synthesis of ZIF-8 membrane for hydrogen separation. Sep Purif Technol 317:123871. https://doi.org/10.1016/j.seppur.2023.123871

Shariatmadari R, Kalaee M, Khajavi R, Shariatinia Z (2023) Novel polyvinyl chloride composite via hybrid metal-organic framework grafted polyethyleneimine and layered double hydroxide incorporation: thermal, rheological, and electrical properties. Alex Eng J 72:225–236. https://doi.org/10.1016/j.aej.2023.03.071

Shi Y, Wu S, Wang Z, Bi X, Huang M, Zhang Y, Jin J (2021) Mixed matrix membranes with highly dispersed MOF nanoparticles for improved gas separation. Sep Purif Technol 277:119449. https://doi.org/10.1016/j.seppur.2021.119449

Shin H, Chi WS, Bae S, Kim JH, Kim J (2017) High-performance thin PVC-POEM/ZIF-8 mixed matrix membranes on alumina supports for CO_2/CH_4 separation. J Ind Eng Chem 53:127–133. https://doi.org/10.1016/j.jiec.2017.04.013

Sultana A, Siddiqui MW, Gaikwad KK (2024) Synthesis of zeolitic imidazolate framework-8 composite as ethylene scavenger for fruits and vegetables preservation and packaging. Biomass Convers Biorefin 14:12725–12729. https://doi.org/10.1007/s13399-022-03066-z

Sutrisna PD, Mustika PCBW, Wijaya C, Putra VIWS, Denaswara PDD, Hadi RP, Widianto AY, Purwanto E (2026) Synergistic effects of combining ZIF-8 and graphene oxide inside cellulose acetate-based mixed matrix membranes on the removal of methylene blue. Case Stud Chem Environ Eng 13:101338. https://doi.org/10.1016/j.cscee.2026.101338

Tian X, Huan H, Zhang K, Zhang R, Liu L, Liu X, Zhang X, Yu Y, Gu T, Wang S, Jiang Z (2025) Building unit engineering toward COF membranes with controlled stacking for H_2 purification. Adv Mater 37:2504622. https://doi.org/10.1002/adma.202504622

Tiemblo P, Saiz E, Guzmán J, Riande E (2002) Comparison of simulated and experimental transport of gases in commercial poly(vinyl chloride). Macromolecules 35:4167–4174. https://doi.org/10.1021/ma011908s

Ul Haq I, Li SH, Zhen HG, Khan R, Zhang AS, Zhao ZP (2021) Fabrication of zeolitic imidazolate frameworks based mixed matrix membranes and mass transfer properties of C_4H_6 and N_2 in membrane separation. AIChE J 67:e17114. https://doi.org/10.1002/aic.17114

Usman M, Suliman MH (2023) Silver-doped zeolitic imidazolate framework (Ag@ZIF-8): an efficient electrocatalyst for CO_2 conversion to syngas. Catalysts 13:867. https://doi.org/10.3390/catal13050867

Vu DQ, Koros WJ, Miller SJ (2003) Effect of condensable impurity in CO_2/CH_4 gas feeds on performance of mixed matrix membranes using carbon molecular sieves. J Membr Sci 221:233–239. https://doi.org/10.1016/S0376-7388(03)00245-X

Wang S (2021) Study on fabrication of negatively charged ultrafiltration membranes and its surface modification. Doctoral dissertation, Kobe University. https://hdl.handle.net/20.500.14094/D1008074

Wijenayake SN, Panapitiya NP, Versteeg SH, Nguyen CN, Goel S, Balkus KJ Jr, Musselman IH, Ferraris JP (2013) Surface cross-linking of ZIF-8/polyimide mixed matrix membranes (MMMs) for gas separation. Ind Eng Chem Res 52:6991–7001. https://doi.org/10.1021/ie400149e

Xu D, Hein S, Wang K (2008) Chitosan membrane in separation applications. Mater Sci Technol 24:1076–1087. https://doi.org/10.1179/174328408X341762

Yang Q, Ren S, Zhao Q, Lu R, Hang C, Chen Z, Zheng H (2018) Selective separation of methyl orange from water using magnetic ZIF-67 composites. Chem Eng J 333:49–57. https://doi.org/10.1016/j.cej.2017.09.099

Zakaria NAS, Goh PS, Lau WJ, Arthanareeswaran G, Ismail AF (2026) Antibiofouling plastic bottle-derived PET ultrafiltration membranes spray coated with Ag/TNT for laundry wastewater treatment. J Environ Chem Eng:121517. https://doi.org/10.1016/j.jece.2026.121517

Zhang J, Ali S, Feng X (2025) Highly selective and stable facilitated transport membranes for olefin/paraffin separation. Sep Purif Technol 357:130060. https://doi.org/10.1016/j.seppur.2024.130060

Zhang Y, Jia Y, Hou L (2018) Synthesis of zeolitic imidazolate framework-8 on polyester fiber for PM 2.5 removal. RSC Adv 8:31471–31477. https://doi.org/10.1039/C8RA06414H

Zhao Q, Sun Y, Zhang J, Fan F, Li T, He G, Ma C (2024) Mixed matrix membranes incorporating amino-functionalized ZIF-8-NH_2 in a carboxylic polyimide for molecularly selective gas separation. J Membr Sci 693:122326. https://doi.org/10.1016/j.memsci.2023.122326

Zhong L, Hu YJ, Xing D, Gu HM (2010) Adsorption of methylene blue on colloidal silver—a surface-enhanced Raman spectroscopy study combined with density functional theory calculations. Guang Pu Xue Yu Guang Pu Fen Xi 30:90–94.

Statements & Declarations

Funding

S Hazarika has received support from CSIR New Delhi for CSIR Mission Mode Project grant MMP065202. P. Bora and P. Gogoi have received support from Department of Science and Technology, Government of India for INSPIRE fellowship (grant no. IF200403 (GAP0811) and IF240080 (GAP0851)). C. Bhuyan received support from Council of Scientific & Industrial Research, New Delhi, India for Senior Research Fellowship (Direct) (ID No. 35110313). A. J. Bhuyan received support from Numaligarh Refinery Ltd., Assam for the research grant GPP-0439. This work is supported by Department of Chemicals and Petrochemicals, Ministry of Chemicals and Fertilizers, Government of India for the research grant GPP0373.

Author contributions

All authors contributed to the study conception and design. Methodology, Software, Formal analysis, Investigation, Data curation, Writing – original draft were done by Prarthana Bora: Methodology, Formal analysis, Data curation were done by Ankur Jyoti Bhuyan; Methodology, Formal analysis, Data curation were done by Chinmoy Bhuyan; Methodology was performed by Priyadarshini Gogoi, Investigation, Data curation, Methodology were done by Xianshe Feng; Conceptualization, visualization, validation, supervision, review & editing, Supervision, Project administration, Funding acquisition were done by Swapnali Hazarika. All authors read and approved the final manuscript.

Ethical Approval

This is not applicable.

Consent to Participate

This is not applicable.

Consent to Publish

This is not applicable.

Competing Interests

The authors have no relevant financial or non-financial interests to disclose.

Data availability statement:

All the relevant data have been presented in the manuscript and Supplementary Materials.

Acknowledgements:

Fundings: S Hazarika thanks CSIR New Delhi for CSIR Mission Mode Project grant MMP065202, P. Bora and P. Gogoi thank Department of Science and Technology, Government of India for INSPIRE fellowship (grant no. IF200403 (GAP0811) and IF240080 (GAP0851)). C. Bhuyan thanks Council of Scientific & Industrial Research, New Delhi, India for Senior Research Fellowship (Direct) (ID No. 35110313). A. J. Bhuyan acknowledge Numaligarh Refinery Ltd., Assam for the research grant GPP-0439.

Grants: Authors acknowledge Department of Chemicals and Petrochemicals, Ministry of Chemicals and Fertilizers, Government of India for the research grant GPP0373; and CSIR New Delhi for CSIR Mission Mode Project grant MMP065202.

People: Authors thank Director CSIR-NEIST, Jorhat for encouraging the research group during various discussions.

Supplementary Files

This is a list of supplementary files associated with this preprint. Click to download.

- SupplementaryMaterial.docx